

CACTI Radar b1 Processing: Corrections, Calibrations, and Processing Report

JC Hardin
E Schuman
N Bharadwaj
K Johnson

A Hunzinger
A Matthews
A Varble
S Giangrande

May 2020



DISCLAIMER

This report was prepared as an account of work sponsored by the U.S. Government. Neither the United States nor any agency thereof, nor any of their employees, makes any warranty, express or implied, or assumes any legal liability or responsibility for the accuracy, completeness, or usefulness of any information, apparatus, product, or process disclosed, or represents that its use would not infringe privately owned rights. Reference herein to any specific commercial product, process, or service by trade name, trademark, manufacturer, or otherwise, does not necessarily constitute or imply its endorsement, recommendation, or favoring by the U.S. Government or any agency thereof. The views and opinions of authors expressed herein do not necessarily state or reflect those of the U.S. Government or any agency thereof.

CACTI Radar b1 Processing: Corrections, Calibrations, and Processing Report

JC Hardin, Pacific Northwest National Laboratory (PNNL)
A Hunzinger, PNNL
E Schuman, PNNL
A Matthews, PNNL
N Bharadwaj, PNNL
A Varble, PNNL
K Johnson, Brookhaven National Laboratory (BNL)
S Giangrande, BNL

May 2020

Work supported by the U.S. Department of Energy,
Office of Science, Office of Biological and Environmental Research

Acronyms and Abbreviations

ADI	ARM Data Integrator
AMF	ARM Mobile Facility
ARM	Atmospheric Radiation Measurement
BNL	Brookhaven National Laboratory
CACTI	Cloud, Aerosol, and Complex Terrain Interactions
CSAPR2	C-Band Scanning ARM Precipitation Radar 2
COR	Sierras de Córdoba
CSU	Colorado State University
DOD	data object definition
DOE	U.S. Department of Energy
eRCA	extended relative calibration adjustment
FIR	finite impulse response
GPM	Global Precipitation Measurement satellite (NASA)
HPC	high-performance computing
HSRHI	hemispherical range height indicator
IOP	intensive observational period
KASACR	Ka-Band Scanning ARM Cloud Radar
KAZR	Ka Zenith ARM Radar
KDP	specific differential phase
NASA	National Aeronautics and Space Administration
netCDF	Network Common Data Form
OMT	orthomode transducer
PI	principal investigator
PNNL	Pacific Northwest National Laboratory
PPI	plan position indicator
RCA	relative calibration adjustment
RCS	radar cross-section
RF	radio frequency
RH	relative humidity
RHI	range height indicator
SNR	signal-to-noise ratio
UTC	Coordinated Universal Time
VAP	value-added product
XSACR	X-Band Scanning ARM Cloud Radar
Z _{DR}	differential reflectivity factor
ZPPI	zenith plan position indicator

Contents

Acronyms and Abbreviations	iii
1.0 Introduction	1
1.1 Overview of CACTI.....	1
1.2 CACTI Radar Assets.....	2
1.3 b1 Processing	2
1.3.1 Calibration.....	3
1.3.2 Data Quality Masks.....	3
1.3.3 Data Quality Corrections.....	4
1.3.4 Derived Fields	4
1.4 Radar Performance.....	4
1.5 Scan Strategy.....	5
1.5.1 Standard Scan Strategy.....	6
1.5.2 Agile Scanning	6
1.5.3 Phase Two Scanning	6
2.0 Calibrations and Corrections	7
2.1 Techniques	7
2.1.1 Corner Reflector Calibration.....	7
2.1.2 Relative Calibration Adjustment.....	8
2.1.3 Self-Consistency.....	9
2.1.4 Differential Cross-Calibration.....	10
2.1.5 Differential Reflectivity (Z_{DR}) Correction.....	12
2.2 CSAPR2 Calibrations and Corrections	12
2.2.1 Reflectivity (Z) Correction.....	12
2.2.2 Differential Reflectivity (Z_{DR}) Correction.....	14
2.3 XSACR Calibrations and Corrections.....	16
2.3.1 Radar Constant Correction	16
2.3.2 Reflectivity (Z) Correction.....	17
2.3.3 Differential Reflectivity (Z_{DR}) Correction.....	20
2.4 KASACR Calibrations and Corrections.....	22
2.4.1 Waveguide Blockage Correction.....	22
2.4.2 Reflectivity (Z) Correction.....	23
2.5 KAZR Correction.....	27
2.5.1 Cross-Comparisons with KASACR.....	27
2.5.2 KACR Intermode Comparison.....	29
3.0 Masks.....	30
3.1 CSAPR2 Masks.....	30

3.2	XSACR Masks	31
3.3	KASACR Masks	31
4.0	Derived Fields.....	32
4.1	Specific Differential Phase (K_{DP}).....	32
4.2	Attenuation Correction.....	32
5.0	Processing Architecture	35
5.1	Overall Architecture	36
5.2	Plug-In-Based Architecture.....	36
5.3	Corrections Configuration Files	38
5.3.1	Configuration Index File	38
5.3.2	Processing Configuration File	39
5.4	Data Provenance.....	41
5.5	Parallel Processing	42
5.6	Impact of New Processing System.....	42
5.7	Available Plug-Ins.....	42
6.0	Description of Data Files.....	43
7.0	References	45

Figures

1	DOE ARM CACTI site in Argentina outside Villa Yacanto.	1
2	Radars installed at AMF1 site for CACTI.....	2
3	Radar b1 computational flow graph.	3
4	Timeline of CACTI radars operating status during the campaign, 15 October 2018–30 April 2019.....	5
5	Scan strategy prior to CSAPR2 motor failure.	6
6	Phase two radar scan strategy, valid from around 2 March, 2019 through end of campaign.....	7
7	Corner reflector calibration from raster scans. Panel (a) is the scan without the corner reflector installed. (b) is the result with the corner reflector installed, but blockage in the waveguide. (c) is with the blockage removed.....	8
8	Φ_{DP} reconstruction for self-consistency calibration.	10
9	CSAPR2 daily median RCA values calculated during the CACTI field campaign.	13
10	HSRHI clutter map generated from CSAPR2 using the composite clutter map method in (5).	13
11	CSAPR2 daily median RCA during the CACTI field campaign using a1-level data files and b1-level data files.....	14
12	Daily median Z_{DR} (black dots) for CSAPR2 during CACTI.....	15
13	CSAPR2 daily median a1 Z_{DR} (black) with offwets (blue) and daily median b1 Z_{DR} (green).	15
14	HSRHI of CASPR2 before and after various corrective steps.	16

15	(a) XSACR daily median RCA (gray) during CACTI before the discovery of a changing radar constant.....	17
16	HSRHI clutter map generated for XSACR during CACTI using the composite clutter map method described in (5).....	18
17	Daily median RCA using a1-level XSACR data (gray) and b1-level XSACR data (blue).....	18
18	Reflectivity cross-comparisons between XSACR and CSAPR2 at the COR CACTI site.....	19
19	Distribution of reflectivity cross-comparison differences between XSACR and CSAPR2 using b1-level data during November and December 2018.....	20
20	Weekly median Z_{DR} with offsets calculated using a1-level XSACR Z_{DR} (dots), weekly median b1-level Z_{DR} (squares) and daily media b1-level XSACR Z_{DR} (triangles), colored by standard deviation (must be less than 1).....	21
21	Weekly median Z_{DR} for XSACR during CACTI colored by standard deviation less than 1.....	21
22	Sample HSRHIs from XSACR from (top) a1 Z and Z_{DR} , (middle) b1 Z and Z_{DR} , and (bottom) b1 attenuation corrected Z and Z_{DR}	22
23	Debris removed from KASACR waveguide.....	23
24	HSRHI clutter map generated for KASACR during CACTI using the composite clutter map method in (5).....	23
25	KASACR daily median RCA values calculated during the CACTI field campaign.....	24
26	Daily median RCA values for KASACR using a1-level data (red) and b1-level data (blue).....	24
27	Sub-daily KASACR RCA values (pink and navy) from a1-level data, relative humidity (RH) values from surface statin (RH<90 in brown, RH>90 in green), rain rates from Pluvio data (blue), reflectivity difference between X/KASACR (black).....	25
28	(a) Sub-daily KASACR RCA during full CACTI campaign, colored by relative humidity (RH) greater than 90%. (b) Sub-daily KASACR RCA that pass attenuation filtering and times when RH<90%.....	25
29	Daily median reflectivity cross-comparisons between XSACR and KASACR.....	26
30	Distribution of daily mean reflectivity cross-comparisons of XSACR and KASACR generated from b1-level data.....	26
31	Sample HSRHI scans from KASACR showing a1 reflectivity and b1 reflectivity.....	27
32	KAZR minus KASACR median daily reflectivity offset for all files with the number of points used in comparison greater than 1000.....	28
33	Median reflectivity offset (KAZR-KASACR) compared to reflectivity.....	28
34	Time series of the median daily reflectivity offset (KAZR-KASACR) for files with the number of points used in comparison greater than 1000 and a relative humidity at that time of <90%.....	29
35	GE minus MD median daily reflectivity offset.....	29
36	Histogram of the median reflectivity offset between GE and MD versus relative humidity.....	30
37	CSAPR b1 variables in a sample HSRHI from 11 November 2018 23:41:24 UTC.....	34
38	XSACR b1 variables in a sample HSRHI from 11 November 2018 23:40:43 UTC.....	35
39	Processing architecture of the new plug-in-based processing system.....	37

Tables

1	Radar specifications during the CACTI field campaign.	5
2	Ranges and thresholds used for gate selection during reflectivity cross-comparisons between radars.	11
3	Attenuation coefficients (a,b) used for calculating specific attenuation for each radar.	11
4	Censor map (CMAP) bitfield definitions.	31
5	Classification Mask for CSAPR2 bitfield definitions.	31
6	Coefficients used to calculate specific attenuation, $A_H = \alpha K_{DP}^c$ in b1 processing.	33
7	Available plug-ins.	42
8	CSAPR2 file contents.	43
9	XSACR file contents.	44
10	KASACR file contents.	45
11	KAZR file contents.	45

1.0 Introduction

The U.S. Department of Energy’s (DOE) Atmospheric Radiation Measurement (ARM) user facility deployed a large number of instruments to a region nearby the Sierra de Córdoba mountains in Argentina as part of the Cloud, Aerosol, and Complex Terrain Interactions (CACTI) field campaign (1). During this campaign, four radars were installed at a site outside of Villa Yacanto as shown in Figure 1. As part of a post-campaign effort to improve the usability of these data, a significant activity was undertaken towards the calibration, correction, and improvement of the data quality of these radar datastreams.

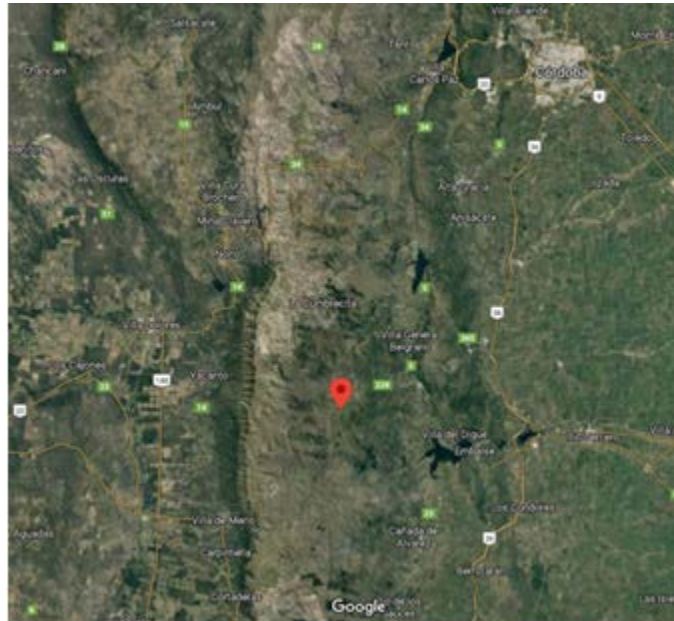


Figure 1. DOE ARM CACTI site in Argentina outside Villa Yacanto.

This process in ARM nomenclature is referred to as generating a “b1” datastream. While these “b1” standards may imply different corrections or standards for various ARM instruments, for radars it refers to a datastream that has been calibrated (and cross-calibrated), including a serious effort to deliver the highest-quality (well-characterized) data possible. This report details (i) the status/quality of the original “a1” (raw) data, (ii) the corrections and calibrations that are applied to generate these b1 datastreams, (iii) the details of the applied algorithms and how radar offset/calibration numbers were determined for the eventual corrections, and (iv) the new and flexible plug-in-based processing system designed during CACTI for radar b1 activities (current, future) that interfaces with ARM’s Data Integrator (ADI) and high-performance computing (HPC) system.

1.1 Overview of CACTI

The CACTI field campaign was “designed to improve understanding of cloud life cycle and organization in relation to environmental conditions so that cumulus, microphysics, and aerosol parameterizations in multiscale models can be improved.”(1) The location was chosen in large part due to the frequent initiation and development of convective storms off the nearby ridgelines. This frequency of convective

initiation makes it practical to capture a large number of storms with a stationary site. The CACTI campaign did not disappoint and sampled a very large number of target cases including more than 100 convective days. As such, the frequency of convection provides a very target-rich data set well suited to the benefits that follow the often time-consuming and labor-intensive efforts required to ensure good calibration and data quality.

1.2 CACTI Radar Assets

Four radars were deployed to CACTI. These included (i,ii) the Ka-Band Scanning ARM Cloud Radar (KASACR) and the X-Band Scanning ARM Cloud Radar (XSACR), a co-mounted, dual-frequency system, (iii) the Ka ARM Zenith Radar (KAZR; a zenith-pointing profiling radar), and (iv) the first deployment of the C-Band Scanning ARM Precipitation Radar 2 (CSAPR2). All radars were installed at the main first ARM Mobile Facility (AMF1) site (labeled COR:M1), as shown in Figure 2. The specifications for the radars are found in Table 1.



Figure 2. Radars installed at AMF1 site for CACTI.

1.3 b1 Processing

It is important to differentiate the algorithms included in b1 processing, and what activities/scope are reserved for downstream value-added products (VAPs) or other user-supported processing (e.g., c1-level, or principal investigator [PI] products). At the outset, several limiting boundaries on b1 processing were established. Overall, the first and most significant limitation is that these processing efforts are restricted to activities constrained by a single instrument. That is, although b1 efforts may consult or perform comparisons against other instruments to obtain information about the corrections for an individual b1 datastream, there is no merging of separate ARM datastreams and/or uses of other instruments at processing time.

There are several different steps in the b1 processing chain. This section covers each of these steps at a high level, before describing various steps in additional detail in the remaining sections of this document. The general flowchart of b1 efforts can be seen in Figure 3.

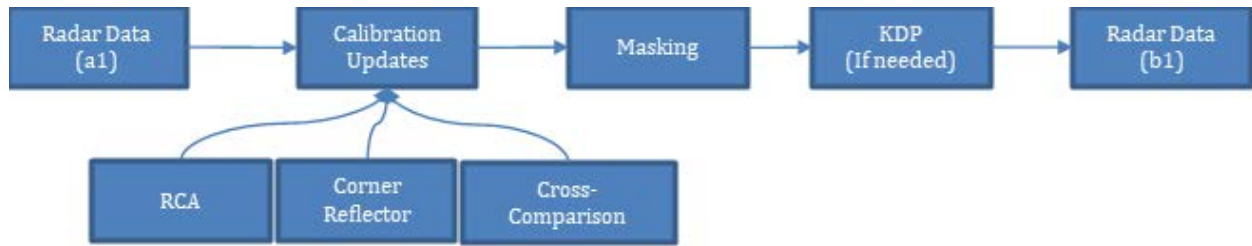


Figure 3. Radar b1 computational flow graph.

1.3.1 Calibration

The primary purpose of the b1 processing is the calibration of the radar datastreams. As will be shown in future sections, there are a variety of ways in which the calibration of a radar can drift. The primary function of calibration is to fix the value of the radar constant C . This constant affects nearly all power measurements the radar takes and represents one of the most dominant sources of errors for the radar. Fundamentally the radar constant is used as

$$Z(r_i) = P_r(r_i) - C + 20\log_{10}(r_i)$$

The radar constant C itself is made up of numerous terms including the finite filter loss, the gain of the antenna, the wavelength, and many others. We can, however, represent it as a constant and, once solved for, correcting calibration is a linear operation for a given time step. This calibration constant exists for both polarizations (where polarization is used) and has a unique value for each. In the case of the KAZR, where pulse compression is used, this has additional terms based on the pulse compression gain. As such, we need to solve for numerous radar constants for each radar. This calculation is also not necessarily constant in time (on longer time scales), as the transmitted power of the radar, the waveguide loss, and many other factors may drift with changes in the environment and radar stability.

For the calibration of the CACTI radars, we have used a wide variety of existing techniques, as well as implemented several new options. These options enable a more robust measure of radar calibration/offset than has been provided for previous ARM campaigns. Additionally, these efforts have heavily used cross-calibration checks with all radars on site and to other-agency partner radars in the area. These ideas extend to satellite overpass concepts, that also help ensure as good a calibration as possible.

1.3.2 Data Quality Masks

The radar measures not only hydrometeors in the atmosphere, but also insects, ground clutter, and extraneous radio frequency (RF) interference. To make the most use of these data, it is useful to construct a series of masks to isolate individual fault conditions in the data. These serve as an index of when data are good or bad, depending on the usage. For instance, a common mask is insects – this is not necessarily an indication of bad data if the user goal is to study clear-air/wind, as insects are often passive tracers of the air motion. Therefore, the application of these masks often depends upon the usage for which they are intended. Because the processing and measured parameters change for each radar, the masks available for individual datastreams will vary from radar to radar.

1.3.3 Data Quality Corrections

In addition to calibration and data quality masks, sometimes there are larger events or circumstances that cause the radar data to be bad/poor. Sometimes, these issues (e.g., complete power/site outage) are not correctable, but in some instances these issues can be remedied. Wherever possible, we attempt to correct for malfunctions or misconfigurations on the radar. For instance, the XSACR during CACTI had a periodic change in the radar constant due to an improperly specified configuration file. These efforts have corrected for these types of issues as much as possible within current resources. When a correction could not be provided, we will attempt to note it in this report.

1.3.4 Derived Fields

To facilitate downstream processing such as VAP and PI product development, it was requested that these b1 efforts include basic derived products within these data. In particular, for the radars that have polarimetry, one addition was to estimate the specific differential phase (KDP) and provide basic corrections for attenuation in rain. Specific differential phase KDP in particular is useful for a wide variety of downstream products, as well as for improved interpretation of the data itself. Attenuation correction in rain provides a measure of the power lost to the environment as the beam propagates through hydrometeors. The efforts have elected to implement simple, well-tested algorithms over potentially better, but less stable, implementations. These fields are not intended to be the best/end estimate for all radar data users but provide a baseline/reference estimate suitable for initial product development. Some users and VAP authors may elect to process these data with more sophisticated techniques, which may be recommended for advanced applications in deep convective cores at shorter radar wavelengths – as common to the CACTI data set.

1.4 Radar Performance

CACTI was a very successful campaign for ARM in terms of radar performance and uptime. This is partially attributed to the conditioning and preparation period for these radar at the Pacific Northwest National Laboratory (PNNL) before the campaign started – where a large number of systems were analyzed, replaced, or upgraded if needed. Thus, the radars were able to capture data over the entire campaign, in a generally good state. Shown in Figure 4 is the uptime of the radars during CACTI (where the radar is considered “up” if data were produced at any time during that day).

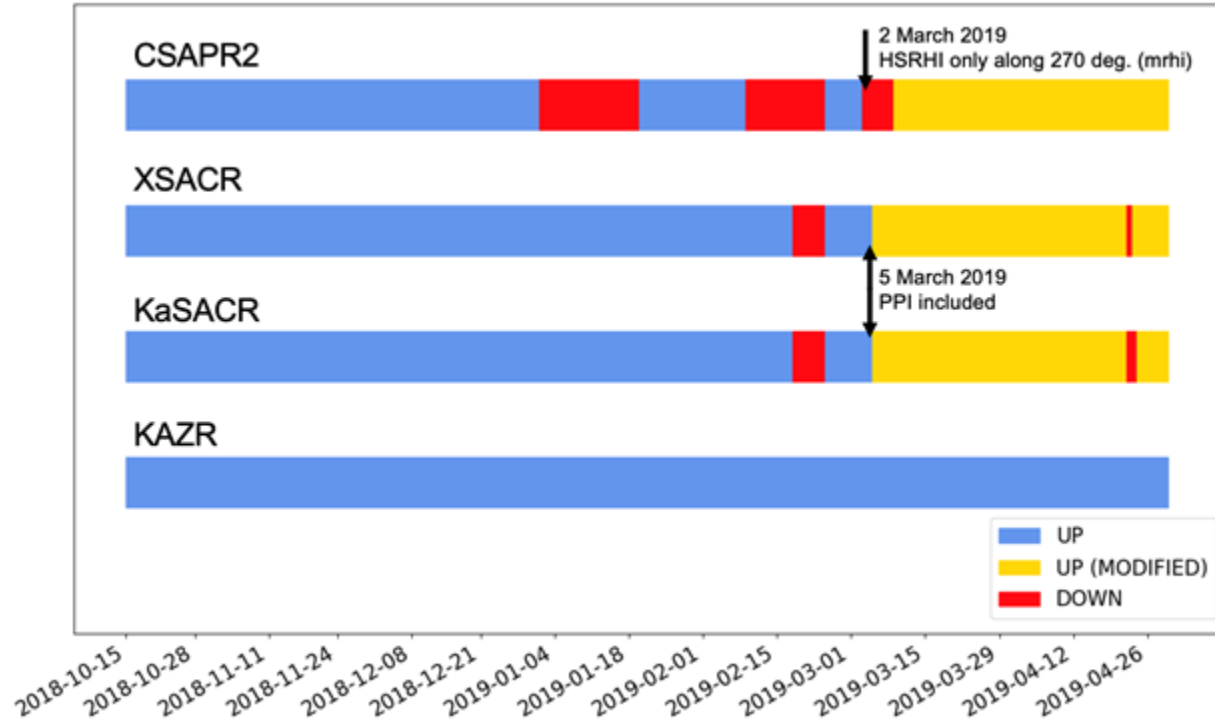


Figure 4. Timeline of CACTI radars operating status during the campaign, 15 October 2018–30 April 2019.

However, during the campaign, the radars did encounter various issues causing periodic downtime, as shown in red in Figure 4. There was downtime for the CSAPR2 around the turn of the year, resulting in a period of no data. Beginning in February, there were additional issues with the pedestal on the CSAPR2. Ultimately, this resulted in failure for the ability to scan this radar in azimuth. As a result, campaign PIs and ARM redesigned CSAPR2 scan strategies to include plan position indicator (PPI) scans on the Scanning ARM Cloud Radar (SACR), while performing a single azimuth range height indicator (RHI) scan with a very high update rate (45 seconds) on the CSAPR2. The period with modified scan strategies is denoted in yellow in Figure 4.

Table 1. Radar specifications during the CACTI field campaign.

Radar	Frequency (GHz)	Wavelength (cm)	Transmit power (kW)	Antenna diameter (m)	Beam width (deg)	Gate spacing (m)	Polarization
CSAPR2	5.7	5.26	350	4.3	0.9	100	Dual
XSACR	9.71	3.09	20	1.82	1.4	25, 75	Dual
KaSACR	35.3	0.85	2	1.82	0.33	25	Horizontal
KAZR	34	0.857	0.187	2	0.3	29.98	Single

1.5 Scan Strategy

Due to changes in operational strategy, and failures in the pedestal on the CSAPR2 as introduced above, three distinct scan strategies were used during the campaign.

1.5.1 Standard Scan Strategy

The radar scan strategy for CACTI was designed to maximize the capture of convective initiation, while still providing high-resolution scans in the vertical dimensions as storms pass over the site. Figure 5 shows the original scan strategy for the first months of the campaign. The CSAPR2 is designed to provide spatial context with PPI scans, before transitioning to a zenith PPI (ZPPI) for a vertical profile (and differential reflectivity factor [Z_{DR}] calibration), and then moving to two sets of hemispherical range height indicator (HSRHI) scans that start at 0 degrees azimuth and occur at every 30 degrees in azimuth until the entire domain has been covered. These HSRHI scans correspond to an angular positioning of (0, 30, 60, 90, 120, 150). Due to the hemispherical nature of the scans, this implies an entire 360-degree area is sampled with those six slices.

The KA/XSACR scanning was designed to provide more vertical information/structure for the convective clouds and thus consisted of an RHI sector, followed by three sets of HSRHIs with similar coverage/design as those implemented for the CSAPR2. The scans were also designed to overlap temporally during these HSRHI modes as much as possible through their implementations.

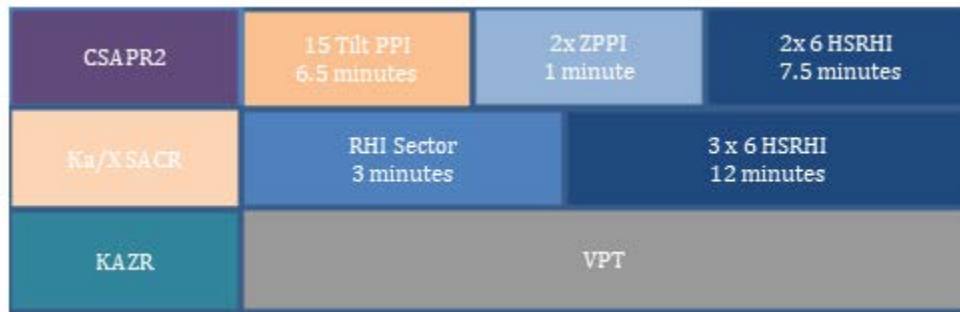


Figure 5. Scan strategy prior to CSAPR2 motor failure. During agile scanning the CSAPR2 HSRHIs are replaced by agile RHIs. This scan strategy was valid from the start of the campaign until about 2 March 2019.

1.5.2 Agile Scanning

During the IOP, occasionally there was a decision to elect to place radars into an “agile scanning” mode, in consultation with the PI/science team for the CSAPR2. During these periods, the radars would switch to a custom-developed scan controller with a command line interface, as well as a custom scan strategy. This scan strategy replaces the 2 HSRHIs with a RHI stack controlled by the operator. The custom controller interface allows the operator to set a few variables (center of scan, scan height, RHI spacing width) and the rest of the parameters are automatically controlled by the system. Therefore, the RHIs during this period can (and will) change from time to time. Otherwise all b1 processing is identical for this period.

1.5.3 Phase Two Scanning

Due to a failure in the azimuth servo motor on the CSAPR2 in late February, the scanning strategies of the radars were reworked. The CSAPR2 was set to a “fast RHI” mode, directed along the 270-degree azimuth, with 45-second heartbeat. This choice was due to CSAPR2 inability to rotate in azimuth. To

maintain a sense of what was happening spatially, a 15-tilt PPI was added to the KA/XSACR while the range was increased to 60 for the XSACR. To keep the heartbeat, this necessitated removing the KA/XSACR RHI sector scan mode, as well as removing one of the HSRHI scan types. The new scan strategy is shown in Figure 6.

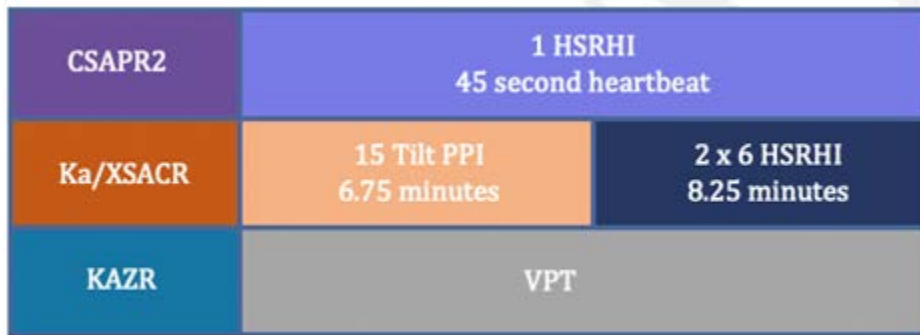


Figure 6. Phase two radar scan strategy, valid from around 2 March 2019 through end of campaign.

2.0 Calibrations and Corrections

Under normal conditions, the calibration of the radars is a multi-part process that consists of several tasks including onsite measurements of transmit power, receiver calibration, and many other tasks. These efforts are typically complemented by a series of calibration scans as partially introduced in previous sections, including birdbath (e.g., ZPPI), scans of a corner reflector, and additional cross-comparisons to ARM and partner radars. Unfortunately, owing to an issue with customs and shipping, the primary calibration equipment for the radar did not arrive on site. In consequence, there was no ability to perform an absolute calibration with RF test equipment.

Due to this limitation, radar calibration had to be based on a series of relative calibrations. This section details the idea behind each measurement/experiment and how it informs the eventual calibration – before presenting the results/summary for these ideas and how they result in the final b1 calibration. Results of this section are fed into the plug-in-based processing system detailed in Section 5.0 and used to process these radar data.

2.1 Techniques

Several techniques are used to calibrate and correct reflectivity-based variables, such as reflectivity and differential reflectivity, for the CACTI radars. The following subsections describe the techniques and how they are applied to the radars.

2.1.1 Corner Reflector Calibration

While many onsite RF measurements are normally done, there is inevitably a portion of the RF chain (nominally, the antenna) that we are unable to calibrate on site. The corner reflector calibration is one method we use to do an end-to-end calibration. Given the transmit power of the radar (which we can measure), we bounce a signal off of an elevated trihedral reflector a distance from the radar. This reflector

has a known radar cross-section (RCS), so we know how much power is expected back at the radar from this reflector. An example of this procedure is detailed in (2). Trihedral corner reflectors are used because of their relative insensitivity to pointing errors. For a trihedral corner reflector with edge length l , we can calculate the maximum RCS as

$$\sigma_{cr} = \frac{\pi l^4}{3\lambda^2}$$

A host of practical issues are known for corner reflector calibrations. For example, these efforts require reconfiguring the signal processor and transmit chain, as well as special processing. In the absence of some of these changes, the error in the corner reflector estimates can be large. In the case of CACTI, corner reflector calibration was performed towards the end of the campaign, but due to the method applied for this processing, the effort resulted in an offset/calibration number that was off by 4 dB based on the analysis on the following sections. This is obviously not adequate for calibration.

These efforts, although not adequate for calibration, did initially point to a significant issue in the KASACR data sets. Moreover, this initial result from the KASACR was much different than expected. After having site operations go through the system, we discovered a blockage had built up in the waveguide. After removal, the numbers matched up better, although still with a 4-dB error that was only discovered much later in post-processing. While this was a useful activity, and one of the few ways ARM has to check calibration end to end, these concepts ultimately proved to be less useful for the CACTI field campaign in terms of establishing b1 calibrations.

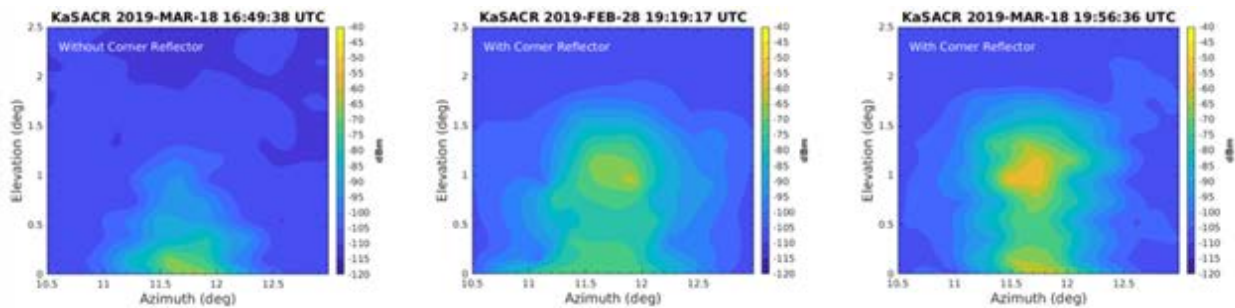


Figure 7. Corner reflector calibration from raster scans. Panel (a) is the scan without the corner reflector installed. (b) is the result with the corner reflector installed, but blockage in the waveguide. (c) is with the blockage removed.

2.1.2 Relative Calibration Adjustment

Even for campaigns featuring viable corner reflector efforts, a proper radar calibration is recommended to provide an operational, online mechanism to monitor the calibration/offsets during the course of the campaign. Previous work in the field (3, 4) has shown that the clutter around a radar can be used as a relative calibration target. This technique, relative calibration adjustment (RCA), does not calibrate the radar directly, but rather monitors how drifts in calibration occur in time. For a complete calibration effort, one can often combine “absolute type” calibrations interwoven with multiple relative calibrations to inform on radar data quality over extended periods. Such combined efforts have not, however, been

validated for higher-frequency (above C-band) radars. As part of these CACTI efforts, ARM activities extended such RCA techniques up through Ka-band radars (5).

One restriction of the previous uses for RCA techniques is that it was initially applied/applicable on PPI modes, which were not available from the SACRs until the end of the CACTI campaign. As part of the current work, additional efforts were performed to extend these techniques to overcome this limitation and allow them to work with RHIs. This new extended RCA (eRCA) technique will form the foundation on which much of this calibration rests. The details of the technique can be found in (5). The technique works by establishing a baseline value on a given day, and then all values are relative to this baseline value.

To interpret the RCA implications on calibration monitoring, one may consider the sign of the RCA value. For example, an RCA greater than zero means that the daily value is less than the baseline value, or the radar is running “cold”. RCA less than zero means the daily value is greater than the baseline value, or the radar is running “hot”. The values are a direct adjustment, which means that by adding the RCA value back into the reflectivity field, you have matched the calibration of that day to the baseline day.

2.1.3 Self-Consistency

After discussions with an outside research group (Dr. Chandrasekar at Colorado State University [CSU]) that performed a comparison of CSAPR2 to the Global Precipitation Measurement (GPM) satellite, it was suggested that the calibration error may be different than was indicated by the initial corner reflector scans. The GPM comparison, however, was only done at one period during the campaign and requires some subtlety to accomplish. We therefore wanted a technique to “break the tie” between the corner reflector and the GPM overpass comparison.

Without the corner reflector as an absolute calibration target, we were forced to look elsewhere for a way to tie the relative adjustments from RCA and cross-comparisons to a single calibration point. One method used in the past has been to compare with a disdrometer, but as the disdrometer for CACTI was co-located with the instruments, this comparison becomes somewhat more difficult and less reliable. One other method that has been used to some success in other projects has been to tie the results of calibration to the internal self-consistency of the dual-polarization measurements (6). This method is not particularly robust and relies on some interpretation (choice of filters) and so is not our first choice but is necessary to determine whether the corner reflector or the single GPM overpass was correct. There are better implementations (namely areal averaging) of this technique, but we elected to go with a simple implementation here just to “break the tie” between the two previous methods.

The self-consistency technique works on the principle that triplets of reflectivity, differential reflectivity, and KDP live in some space that is less than three-dimensional. As such, one can reconstruct one variable based on the other two to some accuracy. Most commonly, this takes the form of calculating FDP along a profile based on reflectivity and differential reflectivity. Then, by comparing the measured FDP profile, and the reconstructed FDP profile, one can determine calibration accuracy.

Ultimately the result of this process confirmed the GPM result (of ~2 dB) for the CSAPR2.

One of the requirements for this technique is a well-calibrated differential reflectivity and differential attenuation correction. In the case here we only chose leading edges of clouds to avoid attenuation and

differential attenuation. This is much easier to accomplish and is shown in Section 2.1.5. As mentioned previously, this is not the most robust technique as implemented here, and we would otherwise not have elected to use it except where we have the secondary comparison with GPM. An example of the reconstruction can be seen in Figure 8.

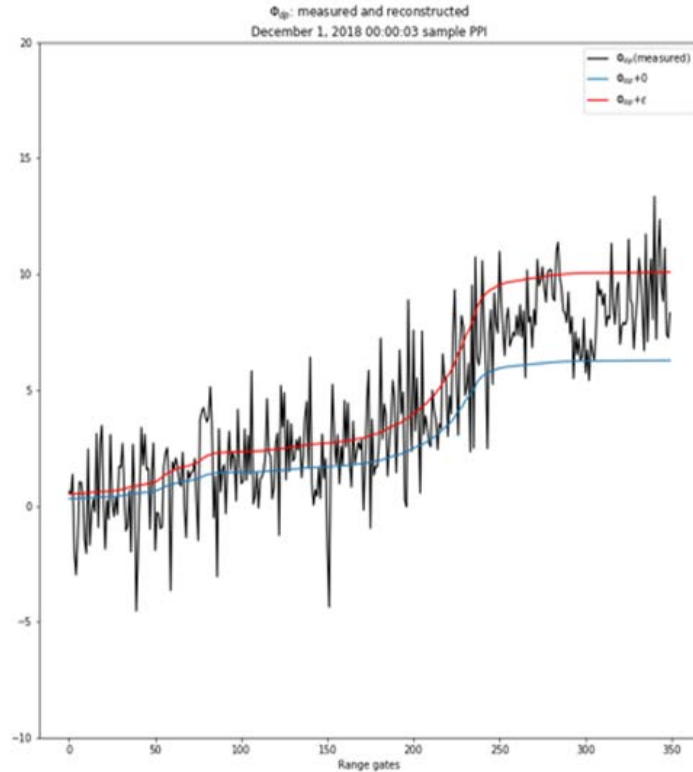


Figure 8. Φ_{DP} reconstruction for self-consistency calibration.

2.1.4 Differential Cross-Calibration

Having confidence in a strong set of 'relative' calibration checks for the CSAPR2 at a point in time (GPM and self-consistency) as a 'absolute' reference, and a way of tracking calibration changes (eRCA), we can then use the CSAPR2 to start calibrating the other radars. This effort takes some care, as the radars are different frequencies, and therefore the measurements of the same target are still expected to differ, even in the case of perfect calibrations.

Differential (cross-radar) calibration requires radar gates from different radars to be matched in space and time to ensure similar precipitation is compared. Co-mounted and co-located radars at the CACTI Sierras de Córdoba (COR) site allowed for reflectivity cross-comparisons. Synchronized scan strategies were designed and implemented to provide as much temporal overlap as possible. Comparisons were performed between CSAPR2 and XSACR, and XSACR and KASACR. Given the varying gate spacing and beam widths of the three radars (see Table 1 for radar specifications), the radar with the smaller beam width and gate spacing is matched to the nearest azimuth, elevation, and range of the radar with the larger beam width and gate spacing. Once radar gates are matched, we filter for conditions of light precipitation. Light precipitation is defined to be low reflectivity ($Z_H < 15$ or 25 dBZ depending on the pair as seen in

Table 2) and meteorological correlation coefficient ($\rho_{hv} > 0.95$). See Table 2 for radar-specific rejection criteria thresholds used for differential cross-calibrations.

Table 2. Ranges and thresholds used for gate selection during reflectivity cross-comparisons between radars.

Radar band comparison	Reflectivity range (Z_H , dBZ)	Correlation coefficient minimum (ρ_{hv})	Elevation range (deg)	Path-integrated attenuation maximum (I_{AH} , deg km ⁻¹)
X - C	-5, 25	0.95	10 - 170	0.1
X - Ka	-5, 15	0.95	10 - 170	0.1

Radar attenuation in rain is a concern for higher-frequency radars, especially when observing heavy rains and severe weather. We performed path-integrated attenuation filtering on XSACR and KASACR. Specific attenuation, A_H , was calculated using a basic relationship with reflectivity:

$$A_H = a Z_H^b$$

where the a and b coefficients differ for each radar (see Table 3). Coefficients were generated based on scattering models using disdrometer data from the site. The absolute accuracy is not particularly important as the corrections are only applied as a filter. Later, a more rigorous attenuation correction pass is applied. Path-integrated attenuation is calculated along each radar ray to estimate the magnitude of attenuation over a certain range. Path-integrated attenuation, I_{AH} , is defined as:

$$I_{AH} = 2 \int_0^r A_H(r) dr$$

Where r is the range at each gate and dr is the gate spacing. This is the cumulative sum of attenuation along a ray going in both the out and back directions (i.e., ‘two-way’, e.g., the multiplication by 2 accounts for this). A threshold of 0.1 deg km⁻¹ for I_{AH} is applied, removing any rays from the comparison that exceed the threshold.

Table 3. Attenuation coefficients (a,b) used for calculating specific attenuation for each radar. Specific attenuation, A_H , defines as $A_H = aZ_H^b$.

Radar band	a	b
C	-	-
X	0.000372	0.72
Ka	0.00115481	0.95361079

Additional filtering is included for KASACR only (the reasoning is described in Section 2.4) with respect to relative humidity (RH) observations near the surface. For times when $RH > 90\%$, KASACR measurements are not included in the comparison.

2.1.5 Differential Reflectivity (Z_{DR}) Correction

Differential reflectivity (Z_{DR}) calibration is performed using vertical, or “birdbath” scans. Traditionally, this form of relative calibration is done using vertically pointing PPIs (i.e., ZPPI) during light rain events. For these efforts, the radar points vertically and rotates a full 360 degrees, yielding 360 rays/profiles for this vertical mode. The Z_{DR} values along these rays are averaged and, because of this selection for light rain (small, spherical drops), the axis ratio of the drops should equal 1, or have a Z_{DR} of 0. The averaged Z_{DR} from the birdbath scan is the offset that needs to be corrected for. This process is generally assumed to be accurate to 0.1-0.2 dB.

HSRHIs were used when birdbath scans were not available for CSAPR2 and XSACR. The birdbath method is modified by choosing the vertically pointing elevation angle(s) (90 degrees, plus 1 degree on either side) of each HSRHI azimuth, and then averaging those rays. A comparison between CSAPR2 PPI birdbath scans and HSRHI scans collected on the same days validated the HSRHI method. While not as robust as true birdbaths, it has been shown in previous calibrations that the results of this have no significant biasing but require a larger number of samples for similar offset estimates.

Daily median Z_{DR} was calculated using each scan in a day and recorded. General offset values were determined for each radar based on the daily median Z_{DR} values in the campaign time series. Details of how the campaign offsets were determined for each CACTI radar are found in the Sections 2.2 for the CSAPR2 and 2.3 for the XSACR.

2.2 CSAPR2 Calibrations and Corrections

Several additional data quality corrections were applied to the CSAPR2 during b1 processing. Differential phase (Φ_{DP}) was flipped during the beginning of the campaign. This was discovered and then corrected on 14 November 2018. The Φ_{DP} sign error has been corrected in the b1 files. Accordingly, K_{DP} and attenuation in rain were recalculated for this period. Details on K_{DP} and attenuation calculations are found in Section 4.0. While the K_{DP} in the CSAPR2 datastreams is correct after this, we elected to reprocess all K_{DP} using the same algorithm to avoid temporal biases in uses of these data.

2.2.1 Reflectivity (Z) Correction

CSAPR2 HSRHI scans were used to calculate RCA values during the entire CACTI campaign. CACTI efforts in (5) validated the use of RHI scans for the RCA method (as above, which was originally conceived for PPI scanning in the previous literature). RCA is calculated for each HSRHI scan in a day, and a median is taken of all scans in that day to yield a daily median RCA value. The daily median RCA values are shown in a time series during the full campaign in Figure 9. Figure 10 shows the locations of clutter points (black) used to calculate CSAPR2 RCA values. Most of the clutter points during CACTI came from the mountains west of the COR site.

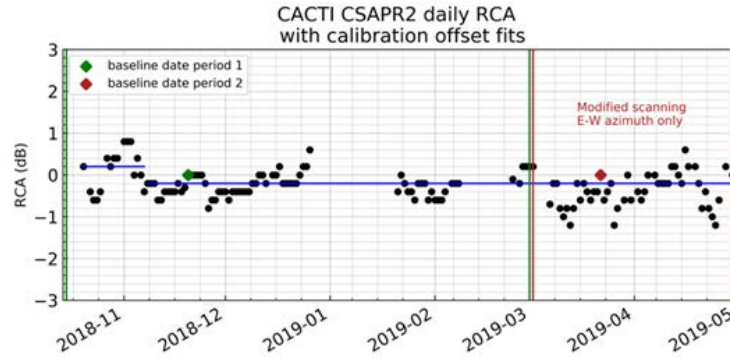


Figure 9. CSAPR2 daily median RCA values calculated during the CACTI field campaign. Black points represent daily median values, while blue lines indicate medians of the daily values that are used as calibration correction values. Two distinct periods were identified.

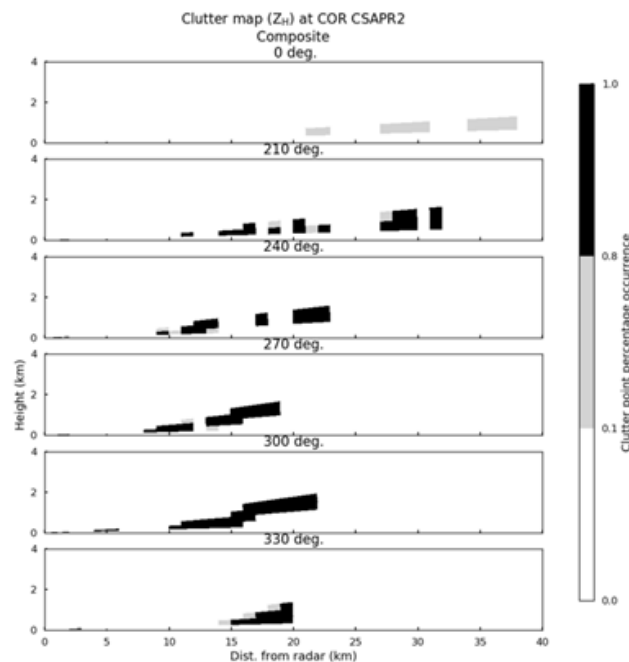


Figure 10. HSRHI clutter map generated from CSAPR2 using the composite clutter map method in (5).

CSAPR2 required two RCA baseline periods (15 October–2 March between the green lines; 3 March–1 May between the red lines in Figure 9). This was because of a mechanical issue the radar suffered, beginning in March 2019. After 2 March, CSAPR2 only scanned along the east-west azimuth (270-90 degrees). During the first baseline period, the daily median RCA values stayed within ± 1 dB, within the margin of uncertainty for RCA. Note again, this is a relative calibration reference at this stage, but provides confidence that the calibration was stable in time (not drifting). Two offset periods were identified (see the two horizontal blue lines) during 15 October–7 November and 8 November–1 May, respectively. After verifying stability of the calibration offset, the correction from GPM and self-consistency ideas suggests that the first offset period has an offset of 2.2 dB, and the second has an offset of 1.8 dB.

Therefore, these campaign offsets were applied during b1 processing to reflectivity for the final correction. RCA was recalculated using the b1-level data and compared to the RCA from the a1-level data as a consistency check. Figure 11 shows the b1-based RCA daily medians in blue, which still fall within +/-1 dB, thus verifying no significant errors in the relative applications of correction factors.

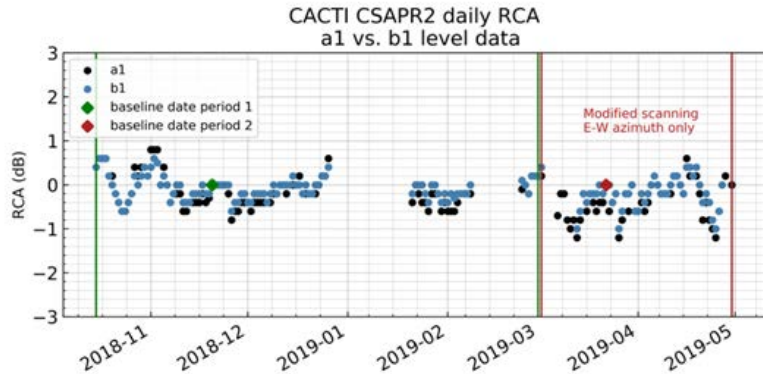


Figure 11. CSAPR2 daily median RCA during the CACTI field campaign using a1-level data files and b1-level data files.

Nevertheless, there is inherent, additional uncertainty in all of the techniques described above. Partially, this uncertainty may be reduced when averaging results over longer periods (at the expense of fine-grained values). As such, an early decision was made to attempt to group calibrations into relatively large temporal periods to avoid chasing statistical uncertainty (attempting to provide detail that were not sustainable under the given methodologies). This decision results in calibration offset corrections having fewer piecewise corrections in time, but perhaps not the best-possible ‘event-to-event’-level calibration details. Note that plots of corrected comparisons will still show some variability for these reasons.

2.2.2 Differential Reflectivity (Z_{DR}) Correction

As mentioned above, the differential reflectivity calibration during most of the campaign was conducted with the traditional “birdbath” vertically pointing scans. Later in the campaign when the azimuth motor failed, we elected to use the HSRHI scans and take rays from within 1 degree of vertical. This shift in method lowers the predictive power of the analysis slightly, and so multiple scans may be required to obtain an accurate Z_{DR} calibration within similar uncertainty bounds. This change in approach has been used and validated in other campaigns and is suggested as not contributing significant bias to the Z_{DR} calibrations or interpretation therein. Since Z_{DR} as a quantity, especially for stratiform/light rain conditions, is relatively robust and not expected to change quickly in time, all of the Z_{DR} calibration numbers are combined into a daily observation. For the majority of the campaign, the Z_{DR} calibration offset was quite stable, with two notable exceptions as shown in Figure 12.

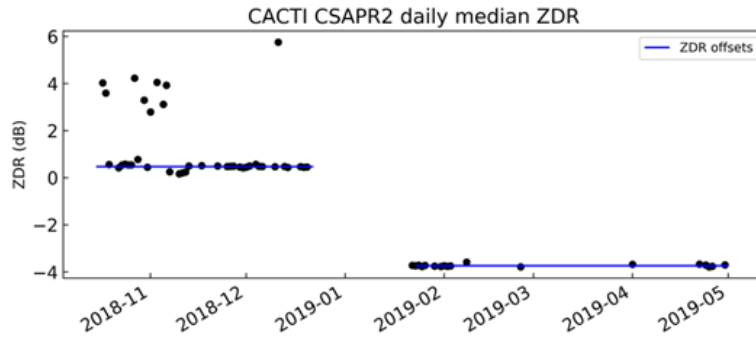


Figure 12. Daily median Z_{DR} (black dots) for CSAPR2 during CACTI. Median offsets (blue lines) are calculated during two periods, 15 October–22 December and 23 January–30 April.

The first and most pronounced exception took place after the radar went down and came back online after the turn of the year. In this instance, the Z_{DR} calibration was significantly reduced (relative shift of approximately 4 dB). Here, we have elected to fit the two periods as piecewise constants (Figure 12). For reference, the first period from 15 October until 22 December had a correction of -0.47 dB, while the second period from 23 January until 30 April had a correction of 3.74 dB. The corrections were applied for the two periods and the analysis rerun. As shown in Figure 13, differential reflectivity is now corrected, with a median of 0 dB.

During the beginning of the campaign, there was an additional and progressive failure of one of the low-noise amplifiers in the system. This caused the differential reflectivity to shift quickly between two stable values (see also, Figure 12, October–November). This can be seen in Figure 13, where some offsets are clear outliers. Unfortunately, as the shift was sub daily and often abrupt (over the course of several scans), we elected not to correct at an individual-file level, and instead correct for the general (global) offset mentioned above. Therefore, care should be taken when using and interpreting files from this period. Additionally, a single day in late February sampled large Z_{DR} values as shown in additional figures below. At this time, there is no obvious explanation for the behavior on this day. After corrections were applied, we reprocessed the analysis to verify the correctness of the data. This new Z_{DR} calibration is shown in Figure 13.

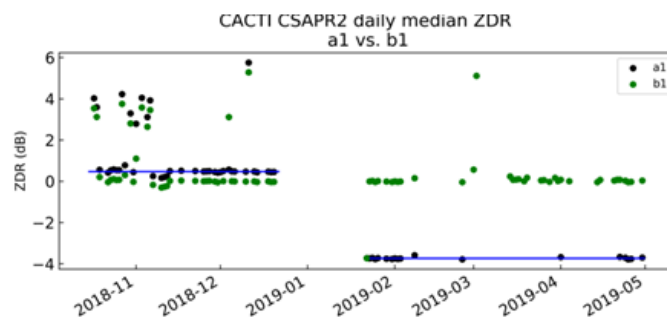


Figure 13. CSAPR2 daily median a1 Z_{DR} (black) with offsets (blue) and daily median b1 Z_{DR} (green).

Finally, to see the effect these calibration changes have on the actual data, we provide a comparison as shown in Figure 14. This image is a HSRHI plot with various parts of the process described above highlighted.

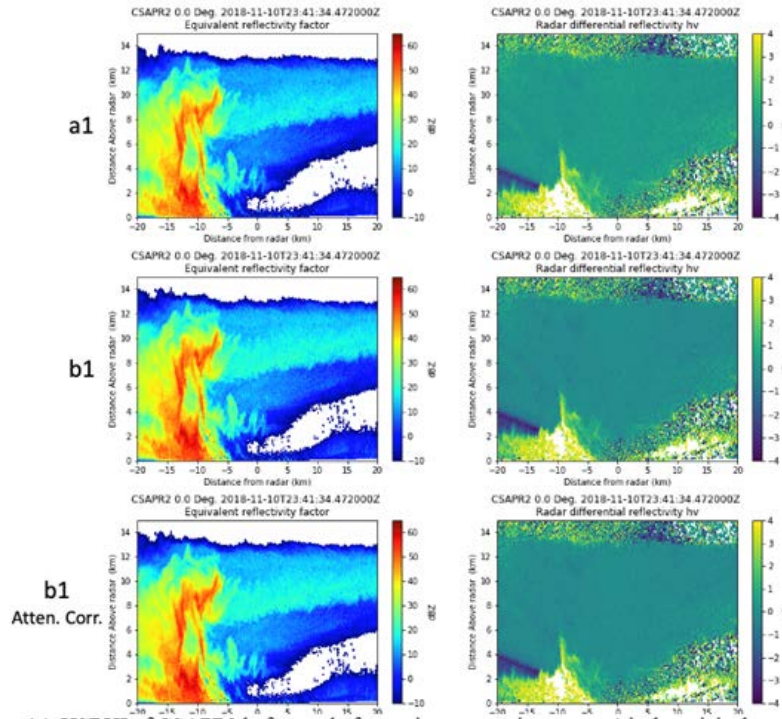


Figure 14. HSRHI of CASPR2 before and after various corrective steps. a1 is the original data, the second row is the data after calibration, and the third row refers to the data after attenuation correction has been run.

2.3 XSACR Calibrations and Corrections

The XSACR operated well over the bulk of the campaign, as previously mentioned. This was partially due to the extended series of maintenance and modifications at PNNL before radar deployment for CACTI. Overall, the primary modifications in b1 were similar to those described above, including calibration correction, masking, attenuation correction in rain, and derived fields.

2.3.1 Radar Constant Correction

The primary method planned to calibrate the XSACR was a combination of RCA, cross-comparisons, and a proxy for absolute calibration. This proxy was originally planned to be the corner reflector, but these ideas were subsequently updated for efforts relying on using polarimetric self-consistency and additional GPM comparisons with CSAPR2.

During the development and testing of these calibration corrections, we noticed piecewise constant periods of calibration that ran the duration of the campaign. It was later discovered that two different radar constants were being input during different periods from the campaign, thus changing the effective calibration by 4.7 dB. This issue was ultimately caused by a workaround in the limitation of the scan controller to perform scheduling for the XSACR that necessitated multiple scan files be created depending on the period the scan was started. On occasion, the technicians would choose the wrong scan file when restarting the radar, i.e., one that had not been updated. ARM has since changed our operating

practice to no longer leave these files accessible for such an issue. For example, this error is revealed clearly in the daily median RCA time series in Figure 15(a).

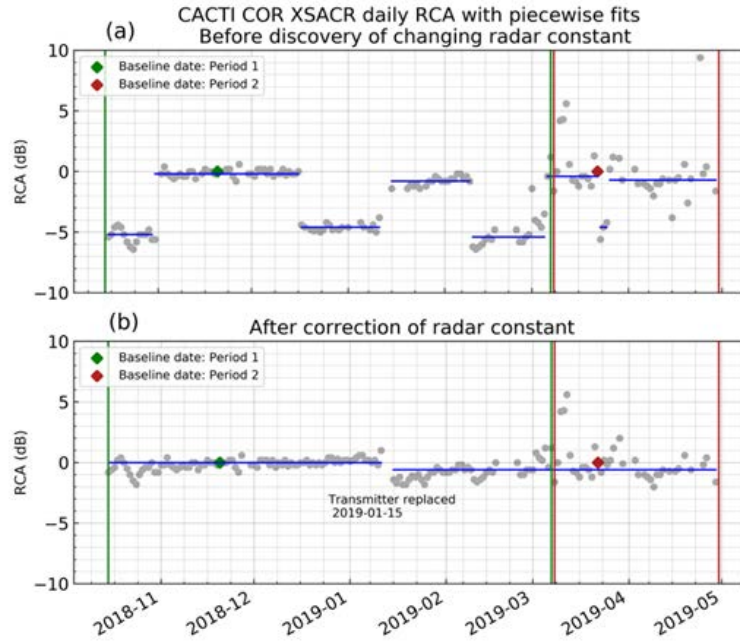


Figure 15. (a) XSACR daily median RCA (gray) during CACTI before the discovery of a changing radar constant. Note the -4.7 dB differences in median offsets. (b) XSACR daily median RCA (gray) after correction of radar constant. Green vertical bars indicate the beginning and end of the first baseline period (15 October–6 March) while red vertical bars indicate the beginning and end of the second baseline period when the gate spacing of XSACR changed the 75 m (7 March–30 April).

RCA values generally fall near one of two averages, the difference of which is roughly the same as the difference between radar constants, 4.7 dB. In order to correct for this, we include a processing step before any corrections are applied that corrects reflectivity for the right radar constant. The correction can be applied as follows:

$$Z_{H \text{ corrected}} = Z_{H \text{ in file}} + (C_{\text{correct}} - C_{\text{in file}})$$

Where C_{correct} is the radar constant known to be correct, and $C_{\text{in file}}$ is the radar constant in the file. As part of b1 processing, the effect of the changing radar constant on the measurements was corrected. Daily median RCA after radar constant correction is shown in Figure 15(b). This correction eliminates the ~5 dB jumps and reveals the relatively stable behavior of XSACR during the campaign.

2.3.2 Reflectivity (Z) Correction

After radar constant correction, the RCA method is used to track the relative XSACR calibration during the campaign. The composite clutter map generated for XSACR using the method developed in (5) is shown in Figure 16.

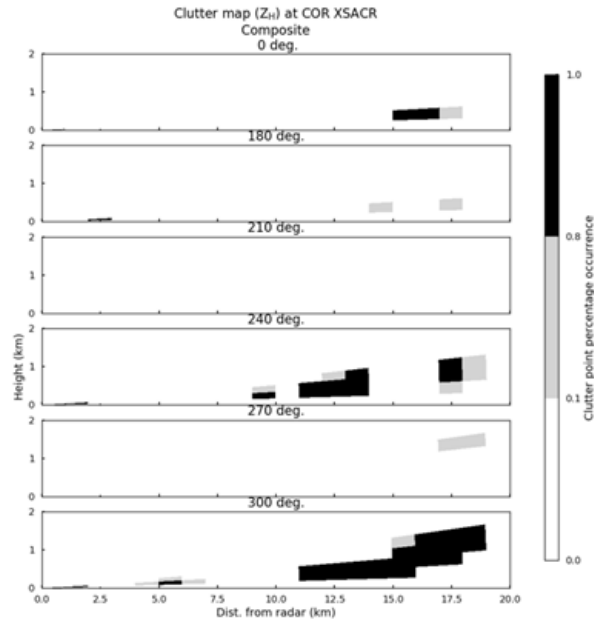


Figure 16. HSRHI clutter map generated for XSACR during CACTI using the composite clutter map method described in (5).

Two baseline periods were used for XSACR. This change was necessitated since the gate spacing was changed from 25 m to 75 m on 6 March 2019 to increase the maximum range. The first baseline period, 15 October 2018–6 March 2019, is shown in Figure 17 between green vertical bars and the second baseline period, 7 March–30 April 2019, is shown between red vertical bars. The XSACR transmitter was replaced on 15 January 2019. Two offset periods were identified based on the hardware replacement done, where the first offset period spans 15 October 2018–12 January 2019 and the second offset period spans 15 January–30 April 2019. RCA values calculated from b1 reflectivity are plotted in blue over the top of the a1 RCA points (gray). The relative calibration of b1 reflectivity remains stable.

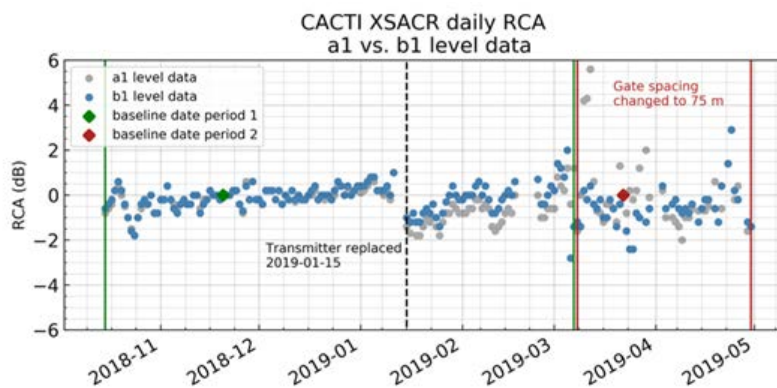


Figure 17. Daily median RCA using a1-level XSACR data (gray) and b1-level XSACR data (blue).

While RCA provides a relative calibration, we still need to tie the XSACR calibration to an external source to provide the “absolute” calibration anchoring. Again, while this anchoring is not truly what is often considered an absolute engineering calibration, the end result is similar. To this end, we performed reflectivity cross-comparisons between co-located XSACR and CSAPR2 radars after the CSAPR2 radar

had been calibrated. This involves matching up periods where HSRHIs are overlapping in time and space. Gates are interpolated to a matched grid, and differenced. Selected points have to match a stringent set of filters designed to reject echoes that are either too strong (i.e., to avoiding non-Rayleigh scattering) or too weak (i.e., to avoid radar sensitivity differences). The median of this process is then calculated for each file, and ultimately reduced down to daily differences.

Figure 18 shows daily median reflectivity differences between matched XSACR and CSAPR2 gates using a1-level data (orange dots), and those from this proposed calibration. Differences between XSACR and CSAPR2 are relatively small (< 2 dB). This give us the difference between the XSACR and a “true” calibration. This, combined with the relative calibration from RCA and the fixes from the radar constant, allows for our eventual calibrated radar datastream. We should note that RCA fixes are not applied at a daily level, but rather as piecewise continuous pieces. We chose this option so as to not introduce any artificial variability from RCA into the datastream.

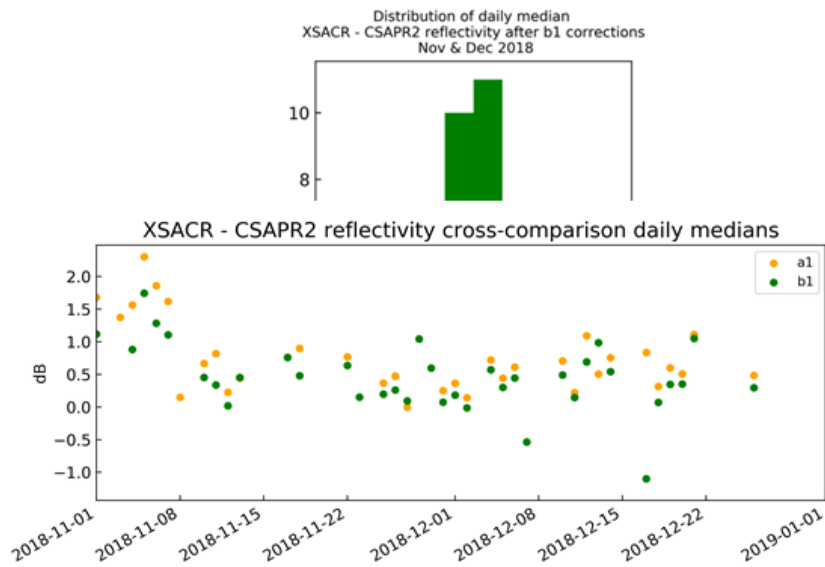


Figure 18. Reflectivity cross-comparisons between XSACR and CSAPR2 at the COR CACTI site.

After correction of b1 data using both cross-comparison and RCA for both radars, the reflectivity difference is calculated again using b1-level data (green dots). Again, differences remain relatively small, though variability still exists. Part of this may be due to the thresholding used in selection of points (see Table 2) for cross-comparison, where different points are chosen for b1 cross-comparison than for a1 comparison. Despite the existing variability, almost all differences in November and December lie within ± 1 dB, as seen in Figure 19.

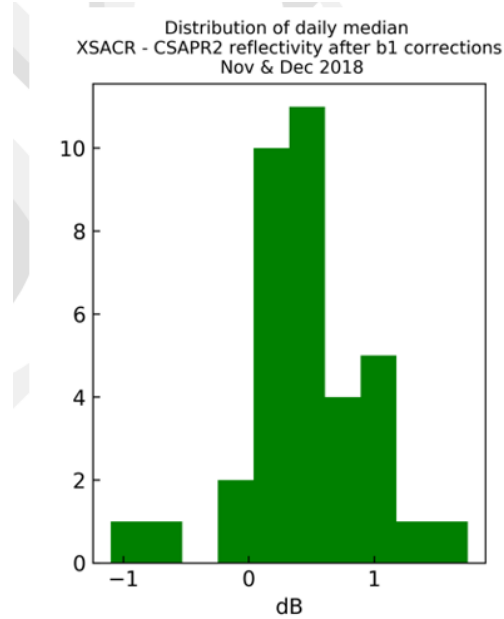


Figure 19. Distribution of reflectivity cross-comparison differences between XSACR and CSAPR2 using b1-level data during November and December 2018.

2.3.3 Differential Reflectivity (Z_{DR}) Correction

As mentioned previously, one can use overhead (birdbath, ZPPI) scans or RHI modes to calibrate differential reflectivity. For RHI modes, recall that this is done by grabbing rays within one degree of vertical and then filtering to acceptable meteorological conditions before calculating a median Z_{DR} . Using this approach, we discovered an error in the ingest that caused the sign of Z_{DR} to be the opposite of the expected value. This is corrected for with an affine transform, multiplying Z_{DR} by -1 in b1 processing.

Once this initial issue was corrected, daily medians of Z_{DR} showed a large variability. However, when calculating the weekly median and filtering for points with standard deviation of less than 1, a more reasonable trend is uncovered. Figure 21 shows weekly median Z_{DR} with offsets marked by blue lines. Two offset periods were identified, using the date of transmitter replacement (15 January 2019) as the divide. Corrections are applied to yield b1 Z_{DR} . The first correction was a constant offset, while the second was a linearly increasing offset denoted by the blue line in Figure 21. The variability in b1 daily median Z_{DR} is still evident (Figure 20, triangles), but the corrected Z_{DR} stabilized when calculating the weekly median (Figure 20 squares), still only using points where standard deviation is less than 1.

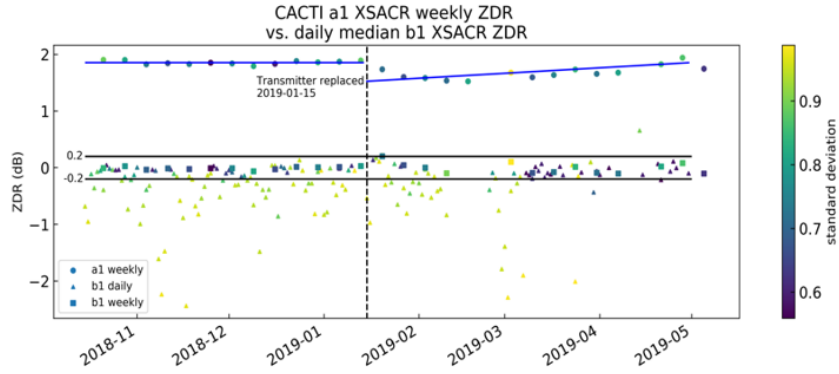


Figure 20. Weekly median Z_{DR} with offsets calculated using a1-level XSACR Z_{DR} (dots), weekly median b1-level Z_{DR} (squares), and daily media b1-level XSACR Z_{DR} (triangles), colored by standard deviation (must be less than 1). Horizontal black lines indicate ± 0.2 dB.

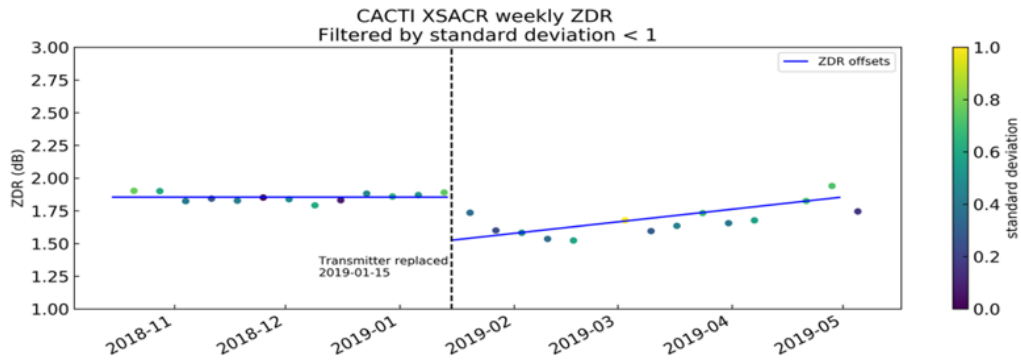


Figure 21. Weekly median Z_{DR} for XSACR during CACTI colored by standard deviation less than 1. The trend of weekly medians with standard deviations less than 1 are used to calculate the offsets (blue lines) during two periods, separated by the replacement of the XSACR transmitter on 15 January.

After correcting for the calibration offsets, the result of the reflectivity and differential reflectivity corrections are shown in Figure 22, comparing a1 to b1 and b1 attenuation-corrected Z and Z_{DR} .

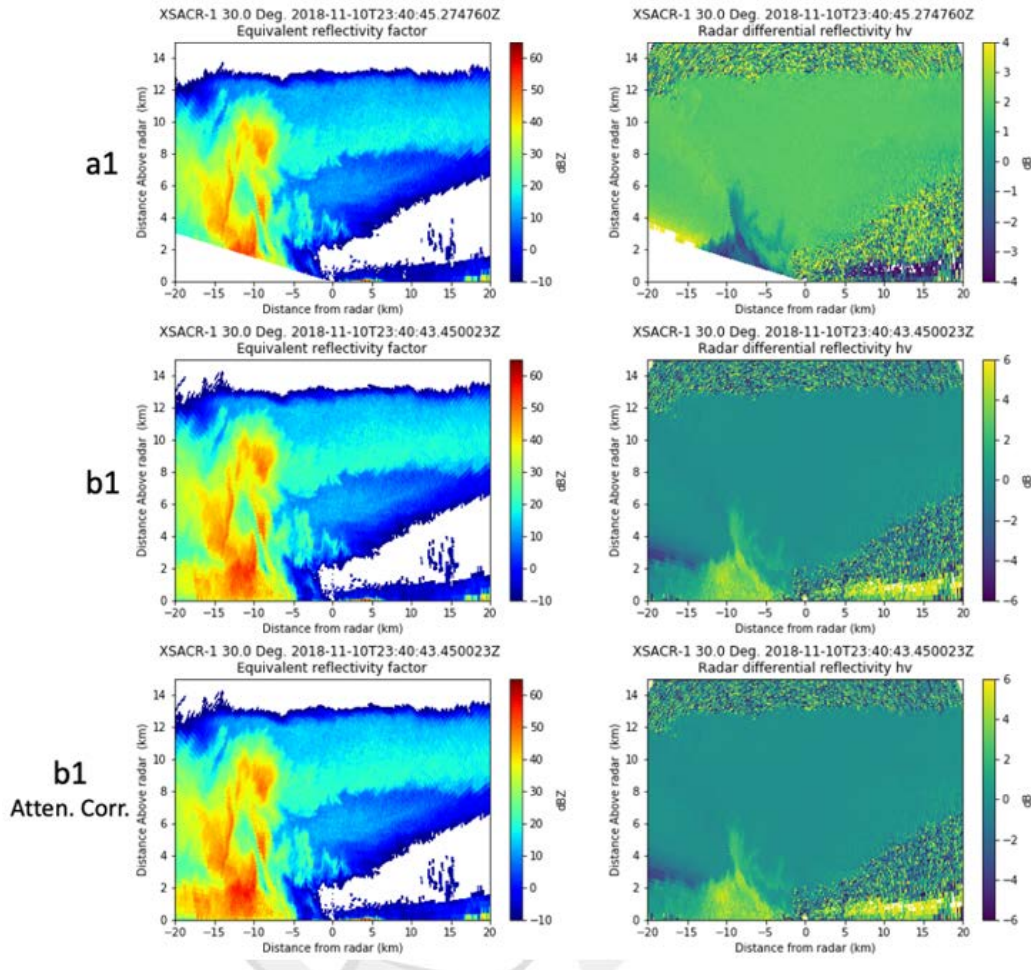


Figure 22. Sample HSRHIs from XSACR from (top) a1 Z and Z_{DR} , (middle) b1 Z and Z_{DR} , and (bottom) b1 attenuation-corrected Z and Z_{DR} .

2.4 KASACR Calibrations and Corrections

Similar to the XSACR, the KASACR operated throughout the campaign and provide good performance up-time, in large part suggested by the similar maintenance and upgrade period at PNNL. The KASACR’s predominant issues that required fixing revolved around the calibration details, mode changes, and select operational problems. There was an obvious issue with waveguide blockage (as mentioned previously and discussed further below), and a known issue with the transmitter losing power during the course of the campaign. This transmitter issue in particular manifests itself as a trend in calibration (fixable), as well as a slowly decreasing sensitivity (non-fixable).

2.4.1 Waveguide Blockage Correction

One major issue that was discovered late in the campaign was debris inside the KASACR waveguide near the orthomode transducer (OMT). This was discovered when the results of corner reflector calibrations were significantly different than expected, as also noted in those sections above. Site operations, upon disassembling the waveguide, noted the debris, falling out of the waveguide as shown in Figure 23. This

debris caused a greater-than-5-dB difference/swing in the calibration. The correction for this issue across the full campaign will be discussed in the next section. The waveguide was ultimately removed and cleaned on 18 March 2019.

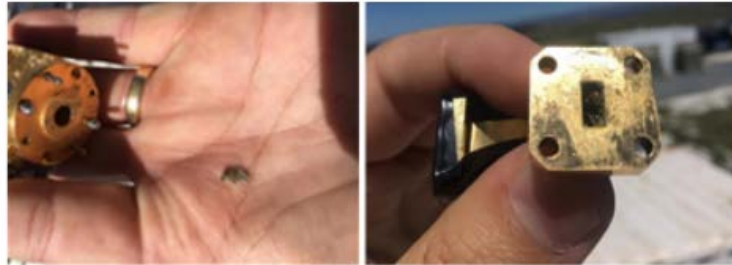


Figure 23. Debris removed from KASACR waveguide.

2.4.2 Reflectivity (Z) Correction

The extended RCA method detailed in (5) was performed on KASACR HSRHIs. The composite clutter map used for RCA calculation is shown in Figure 24. To our knowledge, this is the first time the RCA method has been applied to radar data at this frequency: thus several issues initially arose that required investigation and additional filtering (discussed later in this section). With this additional filtering, we were able to estimate calibration corrections using RCA with confidence.

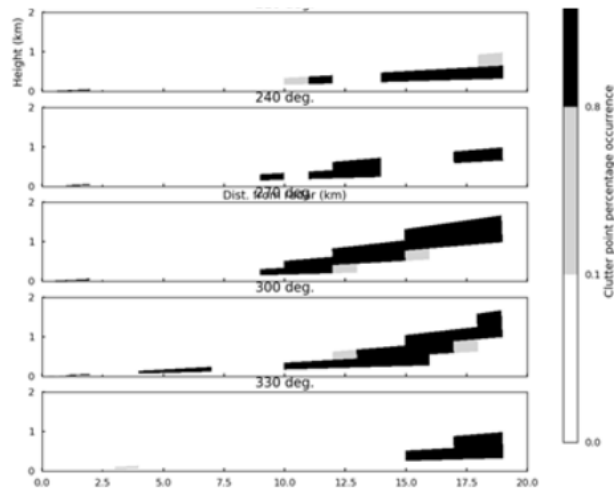


Figure 24. HSRHI clutter map generated for KASACR during CACTI using the composite clutter map method in (5).

Figure 25 shows KASACR daily median RCA after relative humidity and attenuation filtering. Two calibration offset periods were identified, 15 October–17 March and 20 March 20–30 April. These periods are separated by the date of discovery and clearing of debris in the KASACR waveguide (18 March). Each calibration offset period required a polynomial fit to the RCA values, shown by blue and green lines and with the derived fit equations on Figure 25.

Polynomial equations were used to estimate RCA for a particular day, where x is epoch time (time in seconds since 1 January 1970).

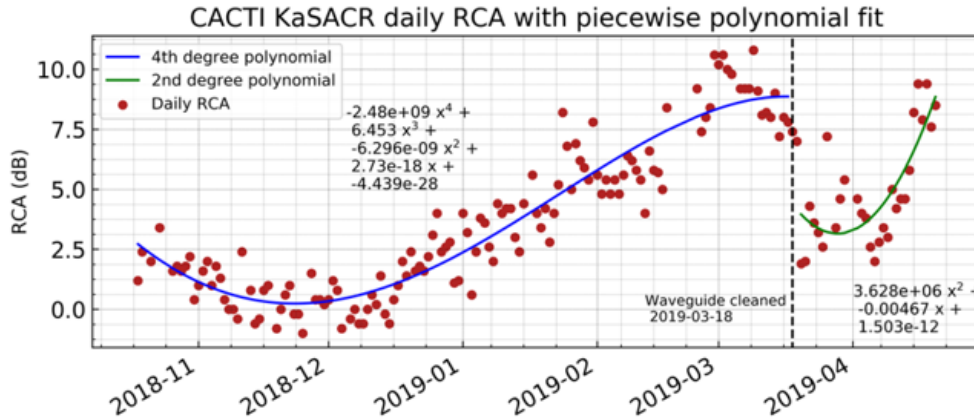


Figure 25. KASACR daily median RCA values calculated during the CACTI field campaign. Red points represent daily median values, while blue and green lines are polynomial fits calculated from daily values, used as calibration correction values. Debris blockage was discovered in the waveguide and was cleared on 18 March 2019, changing the performance of the radar.

Figure 26 shows the improvement of the relative calibration of KASACR reflectivity after applying corrections derived from a1-level data, demonstrated by daily median b1 RCA in blue dots. While variability remains, the large drifts seen in a1 RCA (red) are corrected.

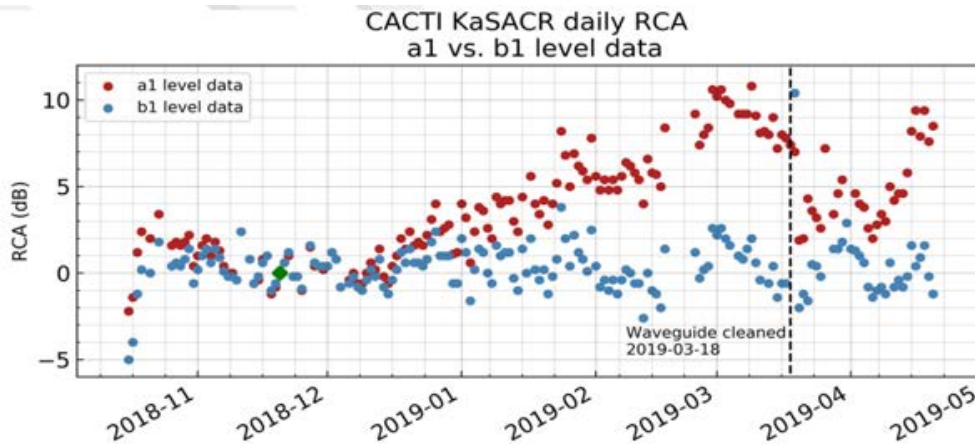


Figure 26. Daily median RCA values for KASACR using a1-level data (red) and b1-level data (blue).

Interestingly, early/morning daily RCA calculations showed widely varying values with no clear trend (e.g., loss of power shown by gradual drifting from 0 dB) or possible explanations for the variability (e.g., hardware replacement). We analyzed a handful of cases at the sub-daily scale, calculating and plotting median RCA for each scan time. Figure 27 shows the sub-daily median RCA, plotted with relative humidity and rainfall measurements from the surface station on site. Because radar at the high Ka-band frequency is known to attenuate easily in heavy rain, a path-integrated attenuation filter was applied while calculating RCA. Pink dots in this figure show RCA values that pass the attenuation filter, while blue dots do not pass the attenuation filter. The blue dots correspond with times of rainfall at the surface near the radar (blue lines, from Pluvio rain gauge data). Relative humidity (RH) is also plotted with RH > 90% in green and RH < 90% in brown. It is clear that the trend of sub-daily RCA followed the trend in RH. This relationship was observed in the other sub-daily cases. Note, for example, after 12Z on 24 January. Here,

in the absence of precipitation, RCA spikes at least 5 dB with a change of only about 10-15% RH. Given the age and condition of the KASACR radome, we suspect that high RH near the surface causes condensation to form on the radome, attenuating the signal (even in the absence of rain). As the radome dries, RCA values return to a stable relative calibration near 0 dB. These values once again spike with increased humidity at later times.

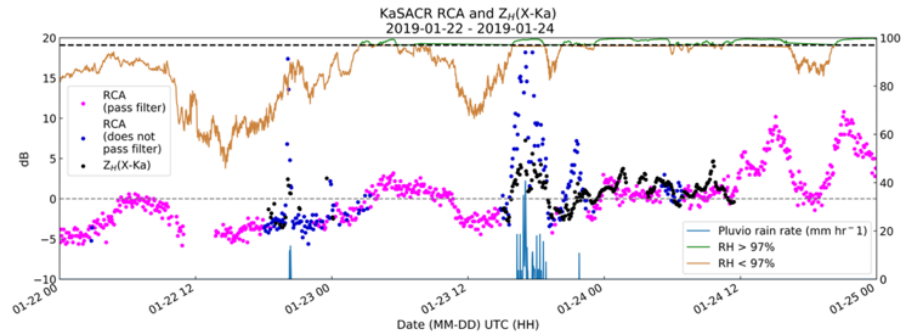


Figure 27. Sub-daily KASACR RCA values (pink and navy) from a1-level data, relative humidity (RH) values from surface statin (RH<90 in brown, RH>90 in green), rain rates from Pluvio data (blue), reflectivity difference between X/KASACR (black).

We investigate this relationship between KASACR sub-daily RCA and RH by visualizing the variability of sub-daily RCA with respect to RH throughout the entire campaign (Figure 28). Before any filtering (attenuation or RH), sub-daily RCA values with RH > 90% (colored dots) stand out as the most wildly varying, reaching up to 25 dB in some cases. Figure 28(b) shows sub-daily RCA after 1) attenuation filtering is performed and 2) scan times when RH > 90% are removed. As a result, sub-daily RCA appears more stable with gentler trends that are better explained by radar hardware issues. 90% is the chosen threshold for RH filtering for KASACR.

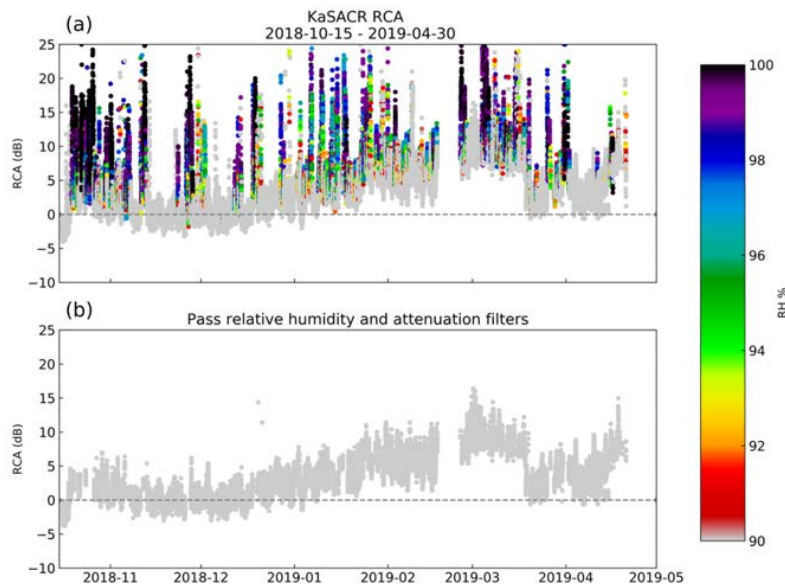


Figure 28. (a) Sub-daily KASACR RCA during full CACTI campaign, colored by relative humidity (RH) greater than 90%. (b) Sub-daily KASACR RCA that pass attenuation filtering and times when RH<90%.

Reflectivity cross-comparisons were performed using co-mounted X/KASACR. Initial cross-comparisons showed daily median differences varying between -2.5 and -7.5 dB, averaging around -5 dB (orange dots in Figure 29). After correcting reflectivity using both cross-comparison and RCA calibration offsets, the cross-comparison between XSACR and KASACR using b1-level data is shown to vary around 0 dB (green dots in Figure 29). Viewing the distribution of the daily median b1 reflectivity differences (Figure 30), almost all points vary within +/- 2.5 dB.

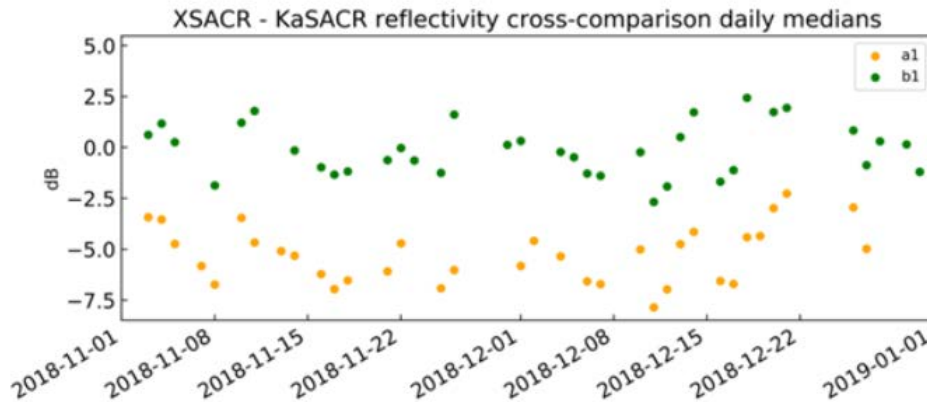


Figure 29. Daily median reflectivity cross-comparisons between XSACR and KASACR. Orange dots indicate reflectivity difference calculated using a1-level data and green dots indicate reflectivity difference calculated using b1-level data.

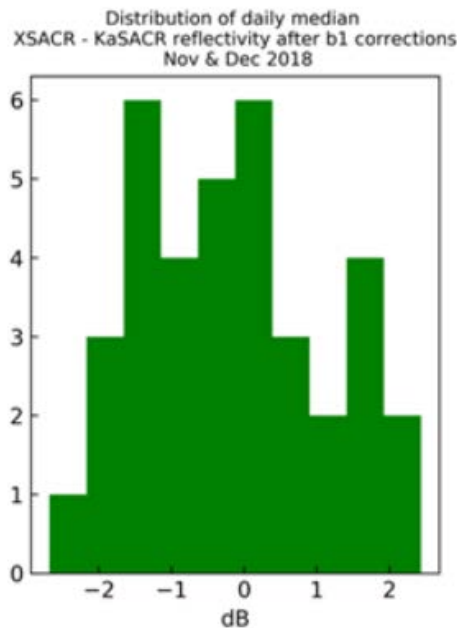


Figure 30. Distribution of daily mean reflectivity cross-comparisons of XSACR and KASACR generated from b1-level data.

The result of all reflectivity corrections applied to KASACR is shown in Figure 31, with a1 reflectivity on the left and b1 reflectivity on the right. This particular scan time is from 3 March, a day when RCA offsets are greater than 10 dB, and the reflectivity correction value applied is 14.5 dB.

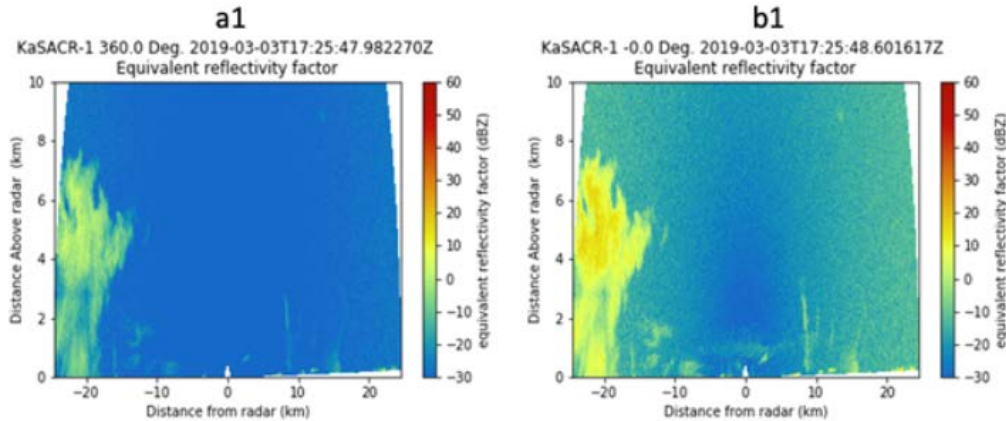


Figure 31. Sample HSRHI scans from KASACR showing a1 reflectivity and b1 reflectivity.

2.5 KAZR Correction

The Ka Zenith ARM Radar (KAZR) is a vertically pointing radar with specifications given in Table 1. It operates using two different pulses. The first is a chirped pulse, referred to as moderate or MD mode, with pulse compression applied to give a much higher level of sensitivity. This does, however, introduce an increased blind range, as the radar cannot see while it is transmitting. There is also short pulse, referred to as general or GE mode, that provides returns closer to the ground. The KAZR at the CACTI site does not have polarimetry. As such, we just need to calibrate the two pulse modes.

There are several methods by which the pulses can be calibrated, and in the process of comparing some of those methods, we uncovered a significant data quality issue in the KAZR datastreams that we note here. For the purposes of this calibration, we compared the KAZR modes to each other (GE and MD) and cross-compared the GE mode with the KASACR and XSACR.

2.5.1 Cross-Comparisons with KASACR

Originally, the KAZR was cross-compared with the KASACR. This was done by using the HSRHI scans from the KASACR after the corrections in Section 2.4 were applied, subsetting these to only pull out the rays within one degree of vertical, and then directly cross-comparing these with the KAZR. The KAZR and KASACR do not have coincident range grids, so to compare the points each KASACR ray was interpolated to a common range grid with the KAZR. Visual inspection of the results showed negligible effect on the actual values due to the interpolation.

Next, we applied a selection filter to the data to control for the differing sensitivity of the radars and selected only good meteorological signal as much as possible. The filters we used were a signal-to-noise ratio (SNR) greater than 0 and reflectivity between -15 and 5 dBZ. Only points that were identified as “good” in both the KAZR and KASACR were used for comparison. A file was output that contained the SACR file date and time, mean offset, median offset, and number of points used in the comparison.

After this file was created, the data were plotted in Figure 32. This plot revealed that a high amount of variability remained after KASACR correction. To understand and mitigate this increased variability, we compared the data with several parameters measured at the site and cross-compared with the KAZR.

After much back and forth, we realized that the variability of this measurement was highly correlated with the relative humidity at the site (see Section 2.4 for a similar analysis for the KASACR). It should be noted that the differences here cannot be attributed to attenuation due to propagation, as the radars are essentially at the same frequency. For similar reasons, the same is true of gaseous attenuation. We currently attribute this variability with humidity to condensation forming on the radomes. To help verify this, we conducted a cross-calibration with the XSACR as compared to both of the Ka-band radars, and saw that both were indeed varying with humidity, and in different proportions. The characterization of the amount and possible correction of this attenuation for the KAZRs will likely be handled in a separate fashion, as it is beyond the scope of this document to account for sub-daily fluctuations. Nonetheless, the difference in the variability in the two Ka-band radars with respect to relative humidity can be explained by differences in the antenna and the motion of the SACR antenna contributing to drop shedding. This work suggests it would be beneficial to update the hydrophobic coating on the radars, which as of this writing are more than 10 years old.

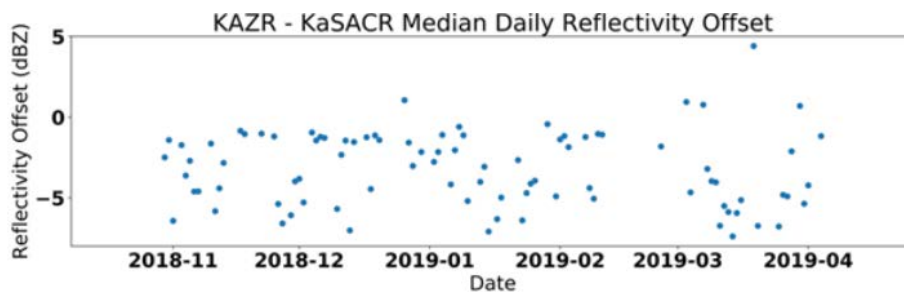


Figure 32. KAZR minus KASACR median daily reflectivity offset for all files with the number of points used in comparison greater than 1000. This shows a high variability day to day, upwards of 10 dB.

The clear effect of humidity on the calculation of the cross-calibration can be seen in Figure 33. Above 90% relative humidity, the variability of the cross-comparison drastically increases. To reduce the scatter, we then filtered the data on relative humidity, removing all data from time periods where the relative humidity was greater than 90%, and reran the analysis.

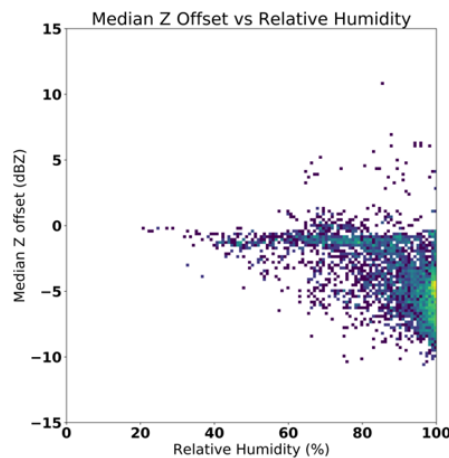


Figure 33. Median reflectivity offset (KAZR-KASACR) compared to reflectivity. There is a high degree of variability present above 90% RH, while the offset is fairly constant at lower relative humidity values.

The plot of the cross-calibration shown in Figure 34 shows the variability is greatly reduced and an offset between the KAZR’s general mode and the KASACR can be fit. To do this, we took the binned median of all files with more than 1000 “good” points at each relative humidity between 40 and 60%, where there was minimal variability in the histogram, and then calculated the mean. The resulting offset between the general mode and the KASACR reflectivities at vertical incidence was 1.35 dB.

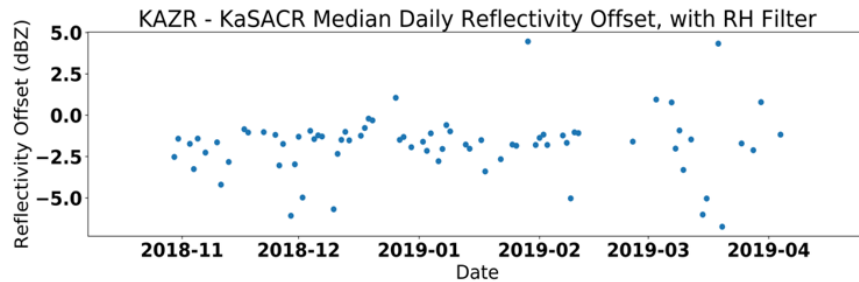


Figure 34. Time series of the median daily reflectivity offset (KAZR-KASACR) for files with the number of points used in comparison greater than 1000 and a relative humidity at that time of <90%. The variability has decreased and a trend is more visible.

2.5.2 KACR Intermode Comparison

Next, the calibration of the general mode can be used as a reference for the comparison with the moderate mode (chirped pulse). We follow a similar method to above to cross-compare the two modes.

First, we interpolated the general mode data to match MD mode. Next, we applied the correction value found above, 1.35 dB, to the general mode reflectivities. The data was then filtered for SNR greater than 0 and reflectivity between -15 and 5 dBZ. Only points that were deemed “good” in both the GE and MD data were used for comparison, and a file was output containing the date and time, mean, median, and number of points used for comparison.

Once this file was created, the data were plotted. This plot, Figure 35, shows little variability and creating a histogram of median offset versus relative humidity confirmed there was little dependence on relative humidity, as shown in Figure 36. This is expected, as both modes take the same route through the antenna and radome. We can see a much smaller variability as compared to the cross-calibration with KASACR, which is also expected due to the smaller number of differing factors in this analysis. We then took the median of all files with more than 1000 points used for comparison at each relative humidity between 40 and 60% to be consistent with the method applied when comparing KASACR and KAZR GE reflectivities and found that the mean offset of this was 3.039 dB.

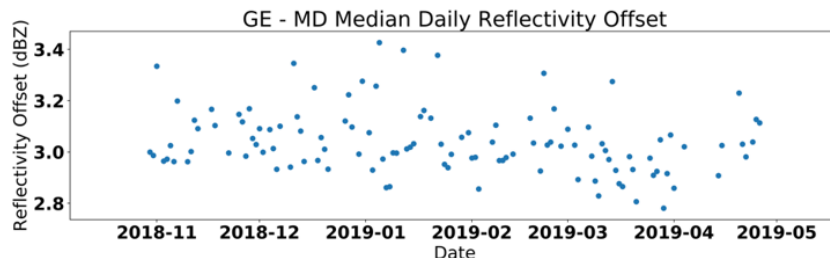


Figure 35. GE minus MD median daily reflectivity offset.

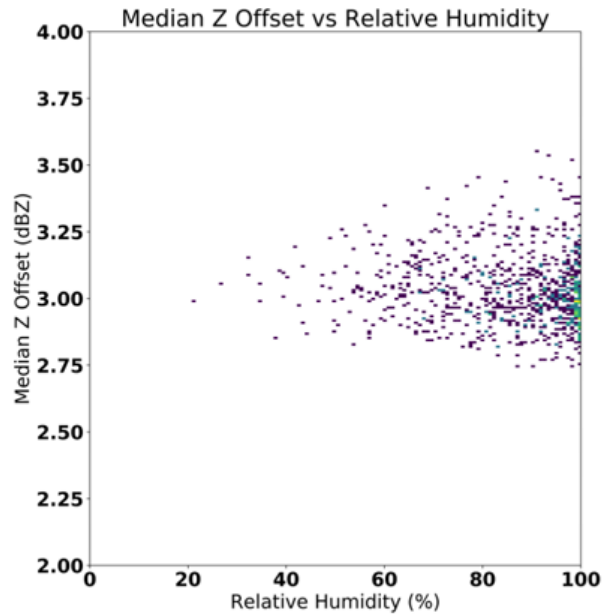


Figure 36. Histogram of the median reflectivity offset between GE and MD versus relative humidity. While there is variability, it is relatively small and not dependent on the RH value.

It should be noted that the analysis here shows why it is **ill-advised to use a disdrometer to calibrate a vertically pointing cloud radar**. As we have shown here, any rain large enough to measure on a disdrometer will cause radome attenuation, making the measurements of the zenith radar no longer comparable with the disdrometer. In our analysis, this is easily upwards of 8 dB. There are also some implications for the sensitivity of the radars being affected by the radome attenuation and what that implies for research into cloud fraction, but that is beyond the scope of this document.

3.0 Masks

3.1 CSAPR2 Masks

The CSAPR2's processing system supplies several built-in masks. These were passed through the b1 system and we will briefly describe them here. There are two mask fields, each with a series of bitpacked individual masks. The following tables are from the manufacturer documentation. The values should, however, be a power of 2 below, and so care should be taken when processing the bitfield.

Table 4. Censor map (CMAP) bitfield definitions.

Value	Name	Description
0x0001	NOISE-H	<i>Is set when the horizontal SNR is below NOISEThreshold</i>
0x0002	NOISE-V	<i>Is set when the vertical SNR is below NOISEThreshold</i>
0x0004	CCOR-H	<i>Is set when horizontal CCOR is lower than CCORThreshold</i>
0x0008	CCOR-V	<i>Is set when vertical CCOR is lower than CCORThreshold</i>
0x0010	SQI1-H	<i>Is set when the horizontal SQI is lower than SQI1Threshold</i>
0x0020	SQI1-V	<i>Is set when the vertical SQI is lower than SQI1Threshold</i>
0x0040	SQI2-H	<i>Is set when the horizontal SQI is lower than SQI2Threshold</i>
0x0080	SQI2-V	<i>Is set when the vertical SQI is lower than SQI2Threshold</i>
0x0100	SIGPOW-H	<i>Is set when the horizontal SIGPOW is lower than SIGPOWThreshold</i>
0x0200	SIGPOW-V	<i>Is set when the vertical SIGPOW is lower than SIGPOWThreshold</i>
0x0400	URHOHV	<i>Is set when UrhoHV is lower than RHOHVThreshold</i>
0x0800	CMS	<i>Censored by Clutter Micro Suppression</i>

Table 5. Classification Mask for CSAPR2 bitfield definitions.

Value	Name	Description
0x0001	SECONDRIP	<i>Is set when range gate has been identified as 2nd trip contaminated</i>
0x0002	THIRDRIP	<i>Is set when range gate has been identified as 3rd trip contaminated</i>
0x0004	INTERFERENCE	<i>Is set when the range gate has been identified as contaminated by RF interference</i>
0x0008	CLUTTER	<i>Is set when the range gate has been identified as contaminated by stationary clutter</i>
0x0010	SUNSPOKE	<i>Is set when the range gate as bee identified as being part of a sunspoke</i>

3.2 XSACR Masks

The XSACR does not contain any built-in masks, so simple masks were added to the b1 files. The two masks consist of a SNR mask that helps to differentiate between returns and noise, and a co-polar correlation coefficient mask. The application of these masks depends on the usage of the data, so no data has been removed, but the masks are available in the file as a first pass at significant echo.

3.3 KASACR Masks

Due to a lack of polarimetry, the KASACR has only the SNR mask added to its data field. The calculation is similar to that from the XSACR.

4.0 Derived Fields

While traditionally secondary derived fields and products are the domain of c1 VAPs, several basic derived fields were added to the b1 ingest to assist downstream processing. The included fields (specific differential phase and attenuation correction in rain) are necessary for basic product development by VAPs, as well as assisting with the use and interpretation of the b1 data itself. The algorithms for these fields were chosen based on their stability, rather than choosing the most novel or sophisticated implementation.

4.1 Specific Differential Phase (K_{DP})

The first derived product is specific differential phase (K_{DP}). This product is used as an input to many different algorithms and techniques in literature. Fundamentally, specific differential phase is the relative shift in the phase of the horizontal and vertical polarizations of the radar with respect to location. It has a close relationship to the amount of liquid in the atmosphere, as well as the attenuation of radar waves as they pass through hydrometeors.

Estimation of specific differential phase can be challenging, as it is not a directly measured quantity by the radar. Radars do measure a related quantity, the total phase shift between the two polarizations, as measured at the receiver with respect to the transmitted waves (often called Ψ_{DP}). It is given by the equation

$$\Psi_{DP}(r) = \int_{r=0}^r K_{DP}(r) dr + \delta_{hv}(r) + \theta_{sys}$$

Where $\delta_{hv}(r)$ is the backscatter differential phase at r , and θ_{sys} is the system phase offset. Essentially, the task is to estimate K_{DP} , which is an integrated forward-scattered quantity, while rejecting the local effect of backscatter differential phase. This is usually accomplished via either some form of filtering (finite impulse response [FIR], adaptive), variational retrieval, or optimization.

In this work, we choose the simplest, but most stable, algorithm for retrieving K_{DP} – namely, the FIR filtering as implemented in (7). While this will not calculate an ideal K_{DP} under all conditions, it is fairly stable and is expected to be sufficient for basic hydrological applications.

4.2 Attenuation Correction

As a radar wave propagates through the atmosphere, it loses some power to the medium (as gaseous attenuation and as attenuation due to hydrometeors). This effect is stronger with stronger storms due to the higher number of hydrometeors in the atmosphere. It is, however, a nonlinear, frequency- and hydrometeor-dependent effect. While attenuation correction is still an open problem in the field, using polarimetry we can approximate the effect in rainy conditions and correct for it.

Similar to specific differential phase estimation above, we will use a basic, but stable, algorithm for attenuation correction in rain. For XSACR wavelengths, gaseous attenuation is assumed to be negligible.

A basic power-law relationship is used to calculate specific attenuation using specific differential phase. The power law is written as:

$$A_H = \alpha K_{DP}^c$$

Where α and c are coefficients that vary depending on radar frequency. The coefficients we used for CSAPR2 and XSACR are found in Table 6, taken from (8). Specific attenuation is not calculated for KASACR as it did not have polarimetry; however, a correction for gaseous attenuation is later included as part of VAP processing for KAZR and KASACR. For the CSAPR2 and XSACR, path-integrated attenuation is then calculated along each ray using the following equation:

$$IA_H = 2 \int_0^r A_H(r) dr$$

Reflectivity is corrected at each range gate, r , by adding the cumulative sum of attenuation (IA_H) at each gate. The equation used is as follows:

$$Z_{H \text{ corrected}}(r) = Z_H(r) + IA_H(r)$$

Table 6. Coefficients used to calculate specific attenuation, $A_H = \alpha K_{DP}^c$ in b1 processing. Coefficients from (7).

Radar band	α (Z)	$c(Z)$	$\alpha(Zdr)$	$c(Zdr)$
C	0.054	1.0	.013	1.23
X	0.25	1.0	.033	1.15
Ka	-	-	-	-

Sample HSRHIs from CSAPR2 and XSACR displaying b1-level radar variables, including the newly calculated K_{DP} and specific attenuation, are shown in Figure 37 and Figure 38. Similar processing was applied to calculate differential attenuation (using different sets of α and c).

Again, no correction for attenuation in rain is made to Ka-band due to the lack of polarimetry, though gaseous attenuation corrections are later applied in subsequent ARM VAP streams.

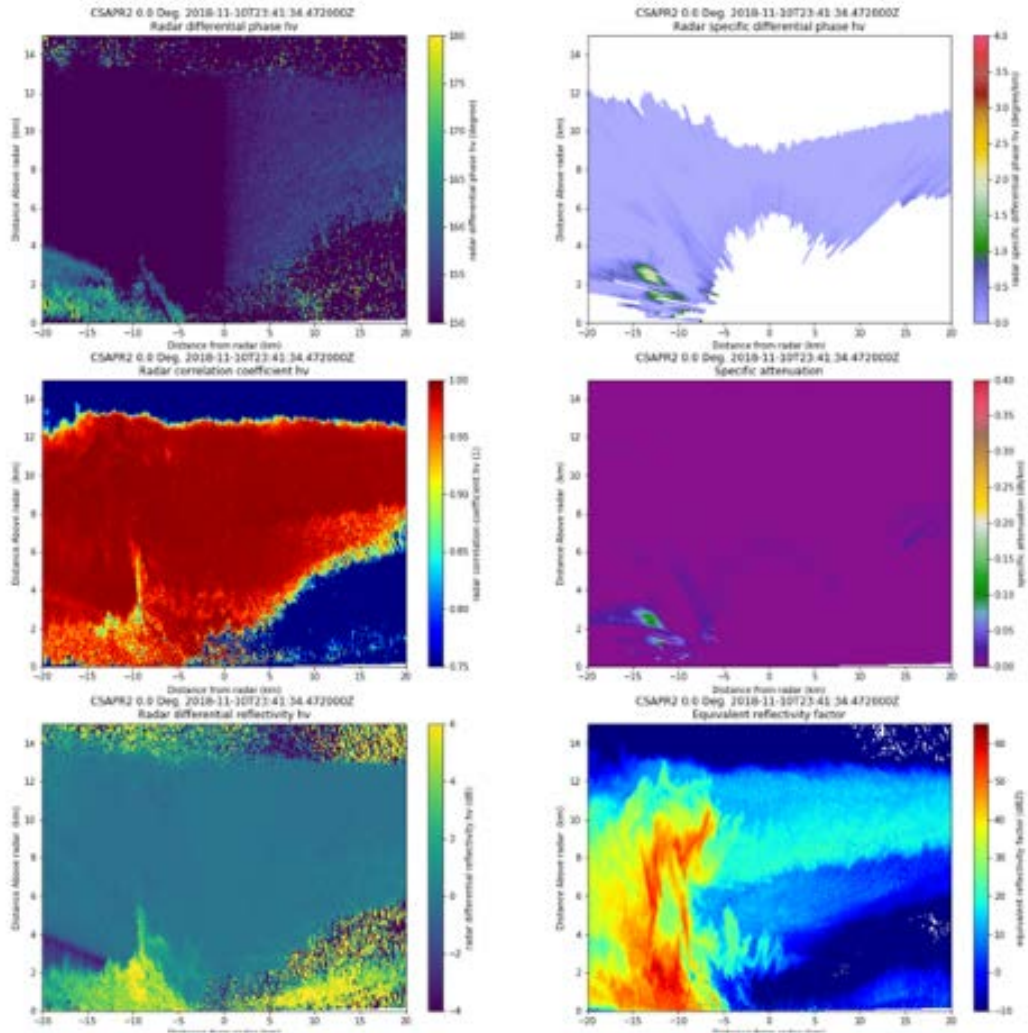


Figure 37. CSAPR b1 variables in a sample HSRHI from 11 November 2018 23:41:24 UTC. Top, left to right: differential phase, specific differential phase. Middle, left to right: correlation coefficient, specific attenuation. Bottom, left to right: differential reflectivity, reflectivity.

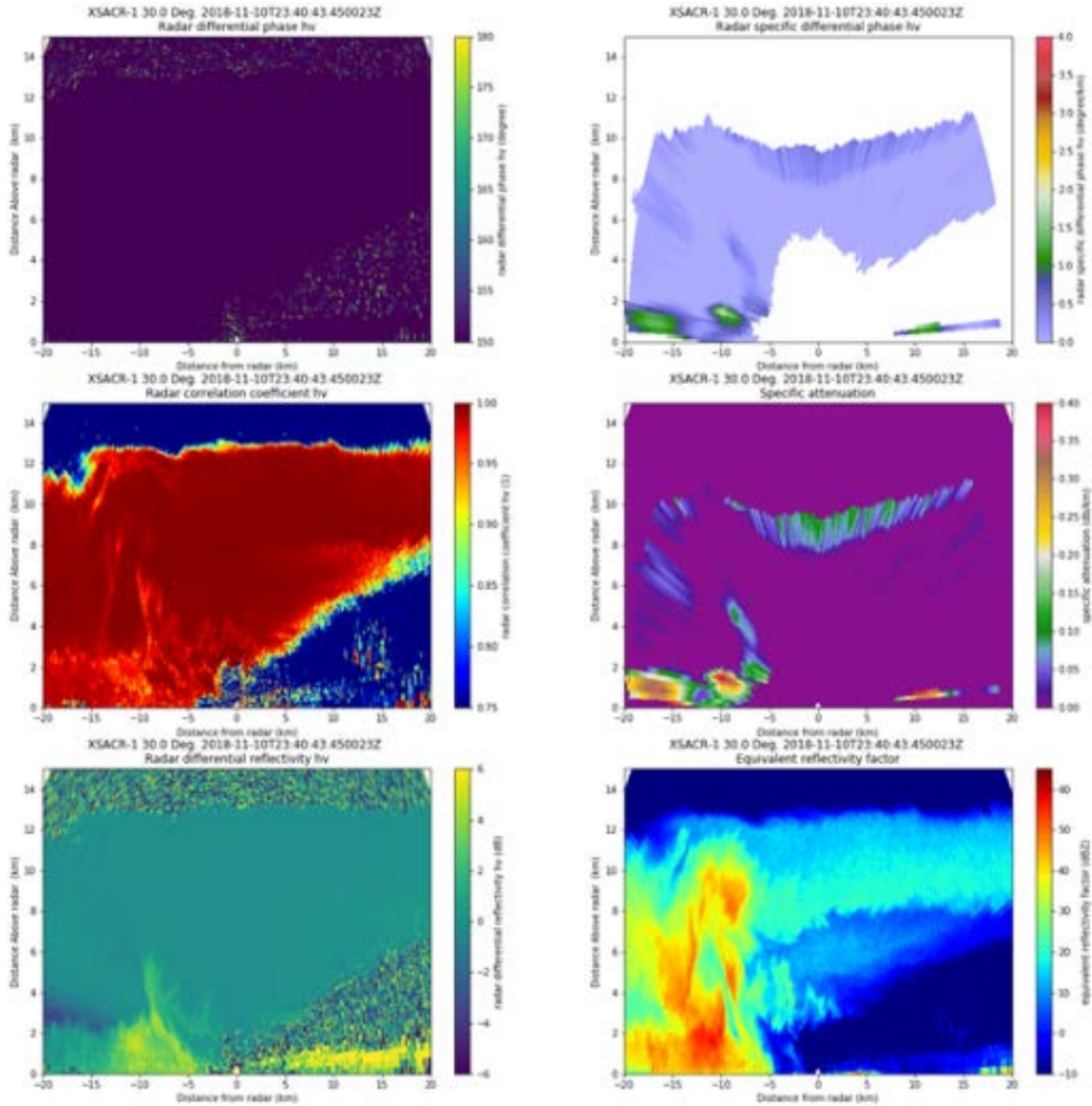


Figure 38. XSACR b1 variables in a sample HSRHI from 11 November 2018 23:40:43 UTC. Top, left to right: differential phase, specific differential phase. Middle, left to right: correlation coefficient, specific attenuation. Bottom, left to right: differential reflectivity, reflectivity.

5.0 Processing Architecture

As part of this project, a new processing system was needed to interface with ARM’s standard data processing system, the ARM Data Integrator (ADI). The existing system works well for typical ARM VAPs and ingests, but certain aspects became a hindrance when dealing with the level of processing needed for this project. We therefore developed a new processing architecture that interfaces with ADI and allows more rapid iterations between the processing and analysis sides of this project. This effort reduced the average time for processing through normal channels from several months to several hours. This fast iteration was critical for testing and development. In the following sections, we go over the new processing system at a high level.

5.1 Overall Architecture

The new “plug-in-based architecture” has several components that work together to simplify b1-level processing for radar datastreams.

The core of the system is still built around the ADI. ADI is used in the ARM data pipeline to retrieve input data, perform checks against ARM standards, and confirm that the data structure matches the structure stored in ARM’s data object definition (DOD) schemas. By using the ADI infrastructure, we are able to ensure that all b1 files meet ARM data standards and simplify the eventual transition of b1 production into operations.

While ADI itself provides many useful benefits, its Python interface is verbose to permit flexibility. As this project was standardizing many parts of the processing, we found it useful to constrain some of this flexibility to simplify operations. In the analysis portion of this project, we used a Python library called ‘xarray’ to access netCDF files, as is common practice in the Python community. To minimize rewriting of code and speed up collaboration between developers and engineers, we wanted to reuse this code inside the b1 ingests themselves. To facilitate this, **we wrote an xarray interface to ADI data structures** (we actually wrote two interfaces but settled on one approach ultimately). This greatly accelerated development and made it simple to interface external libraries into our processing.

With ADI providing the data access, and xarray providing an interface layer, we added a plug-in and configuration system to drive the actual processing. Plug-ins are small snippets of Python code that each conduct one operation. They are given a series of parameters defined by a configuration file and access the xarray radar object. Each plug-in corresponds to one correction applied to the file and is reusable and composable, meaning they can be stacked one after another.

The design and development of a b1 ingest then corresponds primarily to implementing new plug-ins as needed and creating the corresponding configuration files to orchestrate the corrections. This frees those doing the calibration from constant rewriting of code and provides a much easier way of storing historical records of what was done for each b1 processing step. To support this, we also implemented a basic data provenance system within the b1 files, as described below.

5.2 Plug-In-Based Architecture

This section will briefly describe some of the more technical details of the implementation.

The first step is to create a loader to pull the retrieved data from ADI into a standard xarray data set object. The xarray data set gives the development of the corrections more power and flexibility, as developers can leverage the inherent strength of a popular Python data processing library. This also has a side effect that the rest of the plug-in-based architecture can be applied to any xarray data set and is decoupled from ADI-specific implementations.

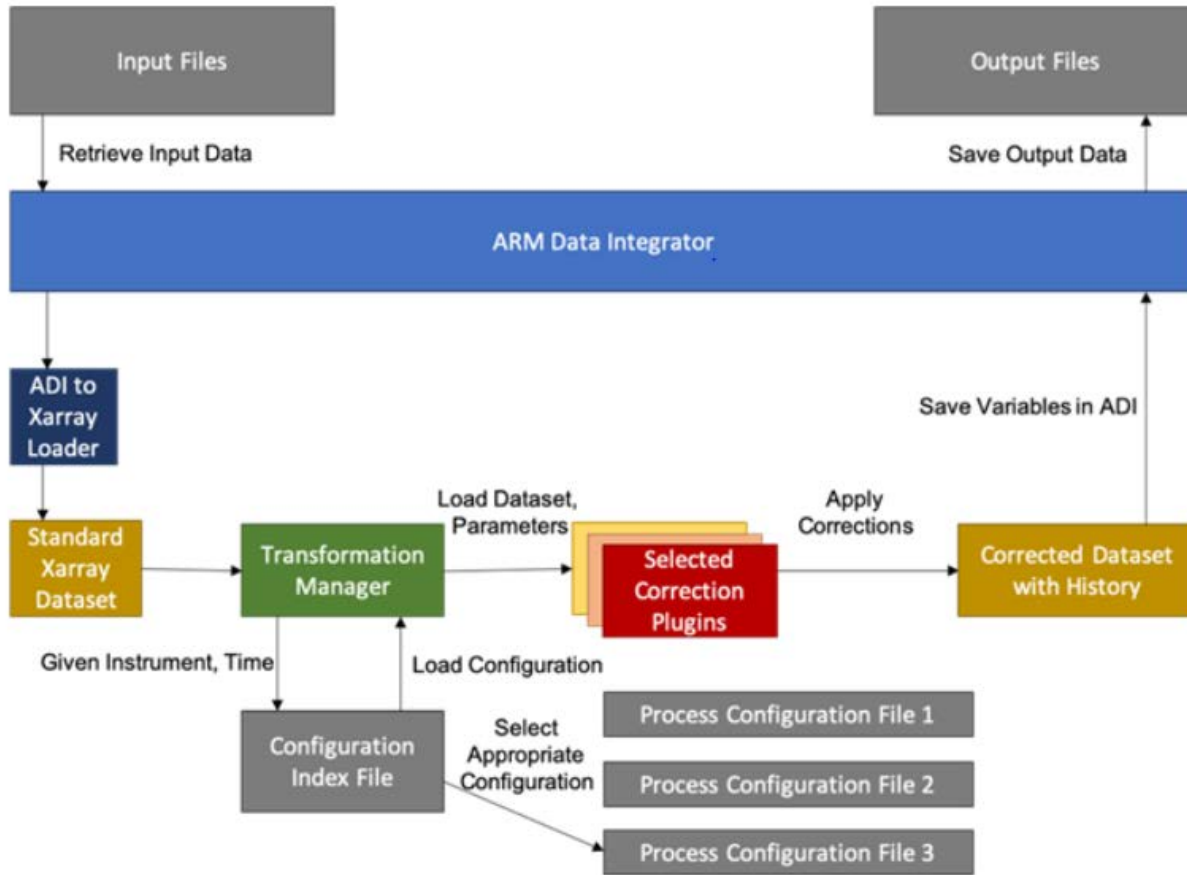


Figure 39. Processing architecture of the new plug-in-based processing system.

Each instrument to be corrected has a set of configuration files which, taken together, define the corrections to be applied, the ordering of the corrections, the scan types involved, and the required time periods. Each of the corrections defined is a combination of a correction name and a set of parameters for the correction.

A TransformationManager is instantiated at runtime, given an xarray data set, a configuration directory, instrument information, and the time of the first sample of the data set. It then parses through the configuration files, building a list of corrections that are relevant to the given instrument at the given time. The TransformationManager contains a mapping of all correction names to a list of defined correction plug-ins. The ingest can then use the new manager to apply the transformations to the given data set. The TransformationManager runs each correction plug-in using its associated parameters in the order specified in the configuration files. It then returns an output xarray data set with all of the corrections applied.

After a new plug-in is created and has implemented all of the expected abstract methods, it only needs to be added to the TransformationManager’s internal mapping, allowing the manager to know what correction name in the configuration files corresponds to the new plug-in. The plug-ins range in complexity from a simple affine transformation of a variable ($\text{variable} * \text{scale} + \text{offset}$, where variable, scale, and offset are the supplied parameters) to the calculation of specific attenuation correction using an

external library. In this case, the plug-in essentially serves as a wrapper to the external code, validating and passing the parameters to the CSU Radartools library (7).

Many corrections that were adjusted and refined over time only required updates to the configuration parameters for the correction. In cases where algorithmic changes were necessary, minimal changes could be made within the relevant plug-in without affecting other plug-ins. This allowed rapid iteration between development and analysis by minimizing and isolating code changes.

As a result, interfacing with ADI for the file retrieval and storage are the only parts handled by the ingest code itself, because all of the transformation logic is self-contained within the b1 transformation library. The configuration is packaged with the ingest, and the b1 transformation library is referenced as a submodule. All of the source code and configuration files are tracked in git and stored on code.arm.gov, so the old versions are always accessible.

5.3 Corrections Configuration Files

The b1 process is orchestrated through a series of configuration files. At a high level, there are two primary types of files used to specify corrections for each b1 file. The first is a site-radar-specific Index File that dictates what correction file(s) to use at which times, and the second is a configuration file that dictates what those corrections are.

5.3.1 Configuration Index File

The first of the two major configuration files is the Index File, where one index file exists per site-radar combination, e.g., for CACTI, there are four index files, one for each radar operated there: csapr2, xsacr, kasacr, and kazr. This file is a YAML file with a simple structure that tracks a set of start and end times, and the corresponding configuration file used to drive that period's corrections. This allows for different sets of corrections to be applied at different times in a campaign, or on different campaigns. The 'start' and 'end' fields contain timestamps, and the corrections for that case will be applied to any data file for that site and instrument whose first timestamp falls between those values. The 'case_label' is used to identify the case to those reading the file but has no bearing on the actual processing. This can be used to denote reasons for choosing the configuration file or labeling of cases or epochs. The 'config_file' is the name of the file that holds the corrections for that particular case.

Below is an example of the index file used for the CSAPR2 during CACTI.

```
corcsapr2_confindex.yml
# One per radar/site.

- 0: # Bad days where Zdr was flipped
  start: 1539561600 # 2018-10-15
  end: 1542153600 # 2018-11-14
  config_file: corcsapr2_proccconf_20181015_20181114.yml
  case_label: "CACTI 0"
- 1:
  start: 1542153600 # 2018-10-15
  end: 1556668800 # 2019-05-01
  config_file: corcsapr2_proccconf_20181114_20190501.yml
  case_label: "CACTI 1"
```

5.3.2 Processing Configuration File

The second major configuration file is the Processing Configuration file. This controls what plug-ins are used and the parameters that control them for processing an a1 file into a b1 file. This is also a YAML file, but with a more hierarchical format. The highest level of the file specifies which datastreams each correction applies to. The ‘datastream’ designation allows individual scantypes (for scanning radars) or operating modes (in the case of KAZR) to be specifically targeted. There is a ‘default’ case that applies to all datastreams (i.e., scantypes or operating modes), but a user may also specify individual datastreams. The second level of the hierarchy is denoted by an ordering number. Each numbered block is a series of plug-ins that applies in the order listed. For each datastream, numbers can be interleaved between the default and the specific datastream. This can be seen in the sample XSACR processing configuration below where the ‘ppiv’ set contains a 3.1. This will be run immediately after step 3 from default, but only for PPIV files. The step numbers can be integer or decimal, and the corrections will be run in the step order, even across scan sections. Within a step block, one or more corrections will be run in the order encountered. The first indent level within each ordered step corresponds to one or more individual plug-in files. So in the corxsacr file below, the plug-in listed in step 1 is ‘radar_constant_correction.’ In step 2, there are three plug-ins: ‘offset_from_file,’ ‘offset_from_file,’ and ‘affine.’. Each correction entry has a name and a set of parameters that will be passed to the correction plug-in.

Many correction adjustments can be made by simply modifying the plug-in parameters, without any need to dig into the source code of the plug-in itself. In the example above, the ‘correct_sweeps’ plug-in is configured differently depending on the type of scan performed.

corxsacr_proconf.yml

```
default:
  1:
    - radar_constant_correction:
      variable: reflectivity
      radar_constant: -20.146378
      radar_constant_name: r_calib_radar_constant_h
  2:
    - offset_from_file:      # Plugin name
      variable: reflectivity
      correction_filename: corxsacr_z_offset.csv
      save_attribute: true
    - offset_from_file:
      variable: differential_reflectivity
      correction_filename: corxsacr_zdr_offset.csv
      save_attribute: true
    - affine: # Correct flipped differential reflectivity
      variable: differential_reflectivity
      m: -1
  3:
    - censor_mask:
      variable: "censor_mask"
      snr_threshold: 0.0
      snr_variable: "signal_to_noise_ratio_copolar_h"
      rhohv_threshold: 0.8
      rhohv_variable: "copol_correlation_coeff"
  4:
    - calculate_kdp:
      variable: "specific_differential_phase"
```

```

threshold: 12.0
window: 5
5:
- calculate_attenuation_correction:
  range_variable: "range" # Gate spacing is attached to the range variable
  uncorrected_reflectivity: "reflectivity"
  corrected_reflectivity: "attenuation_corrected_reflectivity_h"
  specific_attenuation: "specific_attenuation"
  kdp: "specific_differential_phase"
  a: .25
  b: 1.00
- calculate_attenuation_correction:
  range_variable: "range" # Gate spacing is attached to the range variable
  uncorrected_reflectivity: "differential_reflectivity"
  corrected_reflectivity: "attenuation_corrected_differential_reflectivity"
  specific_attenuation: "specific_differential_attenuation"
  kdp: "specific_differential_phase"
  a: .033
  b: 1.15
6:
- rename:
  new_name: "signal_to_noise_ratio_crosspolar_v"
  old_name: "signal_to_noise_ratio_copolar_v"

ppiv:
3.1:
- correct_sweeps:
  fixed_angle: "elevation"
  transition: "antenna_transition"
  start_index: "sweep_start_ray_index"
  end_index: "sweep_end_ray_index"
  decimals: 1
  point_threshold: 0.25
  count_threshold: 50

hsrhi:
3.1:
- correct_sweeps:
  fixed_angle: "azimuth"
  transition: "antenna_transition"
  start_index: "sweep_start_ray_index"
  end_index: "sweep_end_ray_index"
  decimals: 0
  point_threshold: 0.25
  count_threshold: 50

rhi:
3.1:
- correct_sweeps:
  fixed_angle: "azimuth"
  transition: "antenna_transition"
  start_index: "sweep_start_ray_index"
  end_index: "sweep_end_ray_index"
  decimals: 0
  point_threshold: 0.25
  count_threshold: 50

```

This plug-in interface makes it simple for analysts to set up corrections without needing the intervention of a developer. The developer then can spend more time on developing new plug-ins to fix unforeseen issues, rather than setting up routine corrections.

5.4 Data Provenance

Each plug-in run makes some change to a data file. Tracking these changes and recording their provenance is one of the highest priorities, as individual users may not always agree with our choices or may desire to understand exactly what operations were undertaken and their implications.

Each plug-in is expected to implement a function that returns a string describing the changes that the plug-in made to the data set, as well as the specific parameters that were used for the correction. This function is called by the TransformManager as each correction is applied on the data, building a string describing the full history of transformations that were applied to the data. After all the corrections have been applied, this history is stored in the “transform_history” global attribute within the output b1 data set.

A short example of transformation history follows:

```
"Offset from file
\home/user/apps/process/conf/ingest/sacrefrqc/corxsacr_zdr_offset.csv\' applied on
variable(s) \'differential_reflectivity\' of -1.853182406215872 . New attribute saved on
variable.\n",
"Affine transformation applied on variable \'differential_reflectivity\': (var * -1.0) +
0.0\n",
"Variable \'censor_mask\' set as a bit mask. SNR threshold of 0.0 applied based on
variable \'signal_to_noise_ratio_copolar_h\', mask value is 1. RHOHV threshold of 0.8
applied based on variable \'copol_correlation_coeff\' after correction, mask value is 2.
\n"
```

In this example, we see three corrections applied sequentially:

1. The first is an ‘offset_from_file’ with a specified variable name of ‘differential_reflectivity’, a filename ‘corxsacr_zdr_offset.csv’, and ‘save_attribute’ set to ‘true’. The file read the corrections from the given filename relative to the configuration directory, then applied its offset to the given variable name in the data set. It then displayed the offset it applied ‘-1.853182...’ and stated that a new attribute has been saved on the variable. Upon examining the new data set, the variable will have an ‘applied_bias_correction’ attribute attached to it with the correction value recorded.
2. The second is an ‘affine’ transform with a variable of ‘differential_reflectivity’ and an ‘m’ of -1. The ‘affine’ transform accepts parameters of ‘m’ for scale and ‘b’ for offset (following the scheme of $y = mx + b$). ‘b’ is left out, so it defaults to 0 to leave the value unaffected. This correction effectively flips the sign of the ‘differential_reflectivity’ variable in the data set.
3. The third correction is a ‘censor_mask’ transformation. It creates a bitmask that it stores in the variable ‘censor_mask’. It uses a SNR threshold of 0.0, setting the mask if the SNR falls below this value, and it uses the variable ‘signal_to_noise_ratio_copolar_h’ as the SNR variable, setting the mask value as 1. It then does the same thing with RHOHV, with a threshold of 0.8, pulling the variables from the specified variable ‘copol_correlation_coeff’. If a sample is masked, the mask value added is 2.

For each of the plug-ins, it is possible to use the history to see the plug-in used, the parameters used, and a sense for any operations applied to the data. The sample above is pulled from the configuration example

above and shows the last two corrections in step 2 and the full correction in step 3. This provenance tracking makes it easy to track the history of modifications to the file.

It should be noted that many of the plug-ins also indicate the changes they make directly on the variables that are modified, when appropriate. For instance, the calibration correction plug-ins denote the calibration constant applied on the reflectivity variable.

5.5 Parallel Processing

Due to the heavy volume of data involved in processing radar data, a short data processing interval requires significant computational resources. While ADI itself does not support parallel processing explicitly, it does support an asynchronous mode designed to allow for parallel processing controlled by an outside system. We took advantage of this mode to parallelize the processing of b1 data on ARM’s HPC system, Stratus. Processing of individual radar files is independent of each other (often referred to as embarrassingly parallel), so we were able to parallelize the processing by creating a separate ingest process for each core we intended to use. As such, we set up a driver script that broke the job into small pieces, requested a number of nodes from the job scheduler, and then distributed workloads to each of the worker processes in a round-robin fashion.

Using Stratus for multiprocessing, it became possible to process a few days of data in minutes rather than hours, or to run a full campaign for an instrument in hours rather than the months it had previously taken. This in turn allowed for rapid correction adjustment and refinement, as corrections could be quickly applied and the new data analyzed in short order, allowing many more refinement iterations.

5.6 Impact of New Processing System

This new processing system has had an overwhelming impact on the workstyle of the project team. Previously, if data needed reprocessing to fix “minor” issues such as misspellings, unclear descriptions, or anything else that did not have a direct impact on the data, it would be deferred until a larger issue was found. This was due to the large number of resources needed for the reprocessing relative to the gain. With this new system, it has become possible to quickly iterate on large periods of data, find even small issues, and then re-run an entire campaign data set. This has not previously been possible for radar data sets.

5.7 Available Plug-Ins

Table 7. Available plug-ins.

Available Plug-ins	
AffineTransform	Multiply selected variables by a scale factor and add a given offset.
AttenuationCorrectionTransform	Use specific differential phase to correct selected variables for attenuation.
CensorMaskTransform	Create a mask that indicates which samples have SNR or RHOHV fall below a defined threshold.
ClearTransform	Fill selected variables with NaNs or missing values.
CorrectSweepsTransform	Recalculate the sweep start and end indices, as well as setting the flag to mark transition periods.

Available Plug-ins	
KdpTransform	Calculate specific differential phase.
OffsetFromFileTransform	Adds a set of time-dependent offsets from a file to selected variables.
RadarConstantCorrection	Corrects selected variables by adding the difference between the input file's recorded radar constant and the provided radar constant.
RenameTransform	Rename a selected variable.
ThresholdTransform	Threshold a selected variable to a given maximum or minimum value.

6.0 Description of Data Files

This section contains a description of *some* of the more relevant parameters and variables in the radar datastreams.

Key
New variable calculated
Correction applied
New variable and correction applied

Table 8. CSAPR2 file contents.

CSAPR2 File Contents	
Moments	
attenuation_corrected_differential_reflectivity	Differential reflectivity (Z_{DR}) with attenuation correction and offset applied.
attenuation_corrected_differential_reflectivity_lag_1	Differential reflectivity (Z_{DR}) at lag 1 with attenuation correction and offset applied.
attenuation_corrected_reflectivity_h	Horizontal reflectivity with attenuation correction and offset applied.
copol_correlation_coeff	Co-polar correlation coefficient (RhoHV)
differential_phase	Differential propagation phase shift
differential_reflectivity	Differential reflectivity (Z_{DR}) with offset applied.
differential_reflectivity_lag_1	Differential reflectivity estimated at lag 1 with offset applied.
mean_doppler_velocity	Radial mean Doppler velocity, positive for motion away from the radar.
mean_doppler_velocity_v	Radial mean Doppler velocity in the vertical channel, positive for motion away from the radar.
normalized_coherent_power	Normalized coherent power (SQI)
normalized_coherent_power_v	Normalized coherent power, vertical channel
reflectivity	Equivalent reflectivity factor with offset applied.
reflectivity_v	Equivalent reflectivity factor, vertical channel
signal_to_noise_ratio_copolar_h	Signal-to-noise ratio (SNR), horizontal channel
signal_to_noise_ratio_copolar_v	Signal-to-noise ratio, vertical channel
specific_attenuation	Specific attenuation at each bin. Integral of this is applied for correction to attenuation_corrected_reflectivity_h.
specific_differential_attenuation	Specific differential attenuation at each bin. Integral of this is applied for correction to attenuation_corrected_differential_reflectivity.

CSAPR2 File Contents	
Moments	
specific_differential_phase	Specific differential phase (KDP). Calculated using reflectivity, differential phase, and range.
spectral_width	Spectral width
spectral_width_v	Spectral width, vertical channel
Masks	
sensor_mask	Censor mask. See variable details in the files for flags and meanings.
classification_mask	Classification mask. See variable details in the files for flags and meanings.

Table 9. XSACR file contents.

XSACR File Contents	
Moments	
attenuation_corrected_differential_reflectivity	Rainfall attenuation-corrected differential reflectivity with attenuation correction and offset and affine transformation (*-1) applied.
attenuation_corrected_reflectivity_h	Rainfall attenuation-corrected reflectivity, horizontal channel, with attenuation correction and offset applied.
copol_correlation_coeff	Co-polar correlation coefficient (RhoHV)
differential_phase	Differential propagation phase shift
differential_reflectivity	Differential reflectivity (Z_{DR}) with offset applied and affine transformation (*-1) applied.
mean_doppler_velocity	Radial mean Doppler velocity, positive motion away from the instrument.
reflectivity	Equivalent reflectivity factor with offset applied.
signal_to_noise_ratio_copolar_h	Signal-to-noise ratio (SNR), horizontal channel
signal_to_noise_ratio_crosspolar_v	Signal-to-noise ratio, cross-polar for vertical channel
specific_attenuation	Specific attenuation at each bin. Integral of this is applied for correction to attenuation_corrected_reflectivity_h.
specific_differential_attenuation	Specific differential attenuation at each bin. Integral of this is applied for correction to attenuation_corrected_differential_reflectivity.
specific_differential_phase	Specific differential phase (KDP), calculated using reflectivity, differential phase, and range fields.
spectral_width	Spectral width
Masks	
sensor_mask	Bit mask 0: no mask 1: SNR < 0 2: RhoHV < 0.8

Table 10. KASACR file contents.

KASACR File Contents	
Moments	
co_to_crosspol_correlation_coeff	Co-polar to cross-polar correlation coefficient (RhoXH)
crosspolar_differential_phas	Cross-polar propagation phase shift
linear_depolarization_ratio_v	Linear depolarization ratio, vertical channel
mean_doppler_velocity	Radial mean Doppler velocity, positive for motion away from the radar.
reflectivity	Equivalent reflectivity factor, with offset applied.
signal_to_noise_ratio_copolar_h	Signal-to-noise ratio (SNR), horizontal channel
signal_to_noise_ratio_crosspolar_v	Signal-to-noise ratio, vertical channel
spectral_width	Spectral width
Masks	
sensor_mask	Bit mask 0: no mask 1: SNR < 0

Table 11. KAZR file contents.

KAZR File Contents	
Moments	
linear_depolarization_ratio	All values set to nan. This variable is not present in this KAZR.
mean_doppler_velocity	Radial mean Doppler velocity, positive for motion away from the radar.
mean_doppler_velocity_crosspolar_v	All values set to nan. This variable is not present in this KAZR.
reflectivity	Equivalent reflectivity factor, with offset applied.
reflectivity_crosspolar_v	All values set to nan. This variable is not present in this KAZR.
signal_to_noise_ratio_copolar_h	Signal-to-noise ratio (SNR), horizontal channel
signal_to_noise_ratio_crosspolar_v	All values set to nan. This variable is not present in this KAZR.
spectral_width	Spectral width
spectral_width_crosspolar_v	All values set to nan. This variable is not present in this KAZR.

7.0 References

- (1) Varble, A, S Nesbit, P Salio, E Zipser, S van den Heever, G McFarquhar, P Kollias, S Kreidenweis, P DeMott, M Jensen, R Houze, Jr., K Rasmussen, R Leung, D Romps, D Gochis, E Avila, and C Williams. 2018. Cloud, Aerosol, and Complex Terrain Interactions (CACTI) Science Plan. U.S. Department of Energy. [DOE/SC-ARM-17-004](https://doi.org/10.1175/2008JTECHA1063.1), 57.
- (2) Chandrasekar, V, L Baldini, N Bharadwaj, and PL Smith. Recommended Calibration Procedures for GPM Ground Validation Radars, 103.
- (3) Silberstein, DS, DB Wolff, DA Marks, D Atlas, and JL Pippitt. 2008. “Ground clutter as a monitor of radar stability at Kwajalein, RMI.” *Journal of Atmospheric and Oceanic Technology* 25(11): 2037–2045, <https://doi.org/10.1175/2008JTECHA1063.1>

- (4) Wolff, DB, DA Marks, and WA Petersen. 2015. “General Application of the Relative Calibration Adjustment (RCA) Technique for Monitoring and Correcting Radar Reflectivity Calibration.” *Journal of Atmospheric and Oceanic Technology* 32(3): 496–506, <https://doi.org/10.1175/JTECH-D-13-00185.1>
- (5) Hunzinger, A, JC Hardin, N Bharadwaj, A Varble, and A Matthews. 2020. “An Extended Radar Relative Calibration Adjustment (eRCA) Technique for Higher Frequency Radars and RHI Scans.” *Atmospheric Measurement Techniques Discussions*, <https://doi.org/10.5194/amt-2020-57>
- (6) Ryzhkov, AV, SE Giangrande, VM Melnikov, and TJ Schuur. 2005. “Calibration Issues of Dual-Polarization Radar Measurements.” *Journal of Atmospheric and Oceanic Technology* 22(8): 1138–1155, <https://doi.org/10.1175/JTECH1772.1>
- (7) CSU-Radarmet/CSU_RadarTools. 2020. CSU Radar Meteorology Group, https://github.com/CSU-Radarmet/CSU_RadarTools
- (8) Bringi, VN, V Chandrasekar, N Balakrishnan, and DS Zrníc. 1990. “An Examination of Propagation Effects in Rainfall on Radar Measurements at Microwave Frequencies.” *Journal of Atmospheric and Oceanic Technologies* 7(6): 829–840, [https://doi.org/10.1175/1520-0426\(1990\)007<0829:AEOPEI>2.0.CO;2](https://doi.org/10.1175/1520-0426(1990)007<0829:AEOPEI>2.0.CO;2)



U.S. DEPARTMENT OF
ENERGY
Office of Science